Genome-wide profiling of highly similar paralogous genes using HiFi sequencing

Xiao Chen[1], Daniel Baker[1], Egor Dolzhenko[1], Joseph M Devaney[2], Jessica Noya[2], April S Berlyoung[2], Rhonda Brandon[2], Kathleen S Hruska[2], Lucas Lochovsky[2], Paul Kruszka[2], Scott Newman[2], Emily Farrow[3,4,5], Isabelle Thiffault[3,4,6], Tomi Pastinen[3,4], Dalia Kasperaviciute[7], Christian Gilissen[8,9], Lisenka Vissers[8,9], Alexander Hoischen[8,9,10,11], Seth Berger[12], Eric Vilain[13], Emmanuèle Délot[12], UCI Genomics Research to Elucidate the Genetics of Rare Diseases (UCI GREGoR) Consortium, Michael A Eberle[1]

1. PacBio, Menlo Park, CA, USA
2. GeneDx, Gaithersburg, MD, USA
3. Genomic Medicine Center, Children's Mercy Kansas City, Kansas City, MO, USA
4. UMKC School of Medicine, University of Missouri Kansas City, Kansas City, MO, USA
5. Department of Pediatrics, Children's Mercy Kansas City, Kansas City, MO, USA
6. Department of Pathology and Laboratory Medicine, Children's Mercy Kansas City, Kansas City, MO, USA
7. Genomics England Ltd., London, UK
8. Department of Human Genetics, Radboud University Medical Center, Nijmegen, The Netherlands
9. Research Institute for Medical Innovation, Radboud University Medical Center, Nijmegen, The Netherlands
10. Radboud Center for Infectious Diseases (RCI), Department of Internal Medicine, Radboud University Medical Center, Nijmegen, The Netherlands.
11. Radboud Expertise Center for Immunodeficiency and Autoinflammation and Radboud Center for Infectious Disease (RCI), Radboud University Medical Center, Nijmegen, The Netherlands
12. Center for Genetics Medicine Research, Children's National Hospital, Washington, DC, USA
13. Institute for Clinical and Translational Science, University of California, Irvine, CA, USA

Correspondence: Xiao Chen (xchen@pacificbiosciences.com), Michael Eberle (meberle@pacificbiosciences.com)

Abstract

Variant calling is hindered in segmental duplications by sequence homology. We developed Paraphase, a HiFi-based informatics method that resolves highly similar genes by phasing all haplotypes of a gene family. We applied Paraphase to 160 long (>10 kb) segmental duplication regions across the human genome with high (>99%) sequence similarity, encoding 316 genes. Analysis across five ancestral populations revealed highly variable copy numbers of these regions. We identified 23 families with exceptionally low within-family diversity, where extensive gene conversion and unequal-crossing over have resulted in highly similar gene copies. Furthermore, our analysis of 36 trios identified 7 *de novo* SNVs and 4 *de novo* gene conversion events, 2 of which are non-allelic. Finally, we summarized extensive genetic diversity in 9 medically relevant genes previously considered challenging to genotype. Paraphase provides a framework for resolving gene paralogs, enabling accurate testing in medically relevant genes and population-wide studies of previously inaccessible genes.

Introduction

Population-wide whole-genome sequencing (WGS) studies based on short reads have enabled comprehensive characterization of variants, particularly small variants, in ~90% of the human genome (The 1000 Genomes Project Consortium 2015; Bycroft et al. 2018; Karczewski et al. 2020). However, there exist difficult regions and variant classes that remain largely inaccessible to short reads (Mandelker et al. 2016; Ebbert et al. 2019). A large portion of these difficult regions occur within segmental duplications (SDs) (Bailey et al. 2001; Vollger et al. 2022), where high sequence similarity between copies of SDs results in ambiguous mapping of short reads. In addition to difficulty mapping reads within SDs, high sequence similarity promotes unequal crossing over, resulting in hotspots for copy number variants (CNVs), as well as high rates of gene conversion (Chen et al. 2007). These high rates of gene conversion promote sequence exchange between SDs further increasing the errors in read alignment. While short-read based computational methods have been developed to improve the genotyping capability and diagnostic yield in segmental duplications (Handsaker et al. 2015; Ebbert et al. 2019; Prodanov and Bansal 2022; Steyaert et al. 2023), comprehensive variant calling in these regions remains a challenge, and SDs have not been studied at the population level by the current high throughput technologies.

Many medically relevant genes fall into SDs where traditional alignment-based analysis has not been demonstrated to reliably detect the full diversity of these regions. For example, spinal muscular atrophy is caused by variants in the *SMN1* gene, which has a highly similar paralog *SMN2* (Lunn and Wang 2008). Another disease, 21-Hydroxylase-Deficient Congenital Adrenal Hyperplasia (21-OHD CAH), is caused by variants in the *CYP21A2* gene (Merke and Auchus 2020), which resides in a 30-kb tandem repeat called the RCCX module and has a pseudogene *CYP21A1P*. Variants in the *OPN1LW*/*OPN1MW* gene cluster, which contains 1-5 copies of *OPN1LW* or its paralog *OPN1MW*, cause color vision deficiencies (Neitz and Neitz 2011, 2021). To date, these medically important SD-encoded genes are studied with multi-step analyses including a combination of low or medium-throughput assays such as MLPA, amplicon sequencing, or long-range PCR followed by Sanger sequencing to detect copy number (CN) changes or individual variants (Pignatelli et al. 2019; Haer-Wigman et al. 2022). These tests are sometimes limited to a few known variants and may be prone to false negatives if the patient has a pathogenic variant that is not part of the test. There remains a need to fully characterize these genes both for research and clinical testing.

Recently, researchers have begun to study SDs using long-read sequencing. High quality phased assemblies have been generated for a number of samples (Wang et al. 2022; Liao et al. 2023; Gao et al. 2023) using PacBio HiFi and Oxford Nanopore Technologies (ONT) long reads, revealing the sequences of SDs and providing biological and evolutionary insights (Vollger et al. 2022, 2023). However, SDs with multiple copies of highly similar regions are prone to assembly errors especially in regions of extended sequence homology (Vollger et al. 2023). Alternatively, we developed a phasing approach, Paraphase, that identifies haplotypes of genes and their paralogs and demonstrated the ability to accurately resolve the highly similar *SMN1*/*SMN2* region (Chen et al. 2023). That study was limited to one difficult region, leaving a need for a genome-wide demonstration.

Here we extended Paraphase to analyze 316 paralogous genes that fall into 160 groups of SD regions across the genome, including many medically relevant genes that were traditionally considered challenging to genotype. Applying Paraphase to 259 individuals from five ancestral populations, we showed the genetic diversity of these regions across populations in copy number (CN) and sequence variation. We note that some of these regions show exceptionally low diversity between genes and paralogs, signaling high rates of gene conversion. Finally, we studied the Paraphase derived haplotypes for these gene families in 36 parent-offspring trios and identified 11 *de novo* events, among which 7 are *de novo* single nucleotide variants (SNVs) and 4 are consistent with *de novo* gene conversion events.

Results

Profiling 160 gene-coding homologous regions with Paraphase

Paraphase resolves highly similar genes by realigning HiFi reads to one, most relevant, gene chosen to represent all copies of the gene and its paralogs. We call this gene the archetype gene. For example, to study *SMN1* and *SMN2*, we realign all of the reads that are aligned to either *SMN1* or *SMN2* to just *SMN1* because that is the fully functional copy. The aligned reads are then phased into haplotypes for variant calling (Figure 1A). For this study, we identified 160 homologous regions >10kb in length with >99% sequence similarity that were found between two and four times in GRCh38 (Table S1, also see Methods). These homologous regions encode 316 genes in total (excluding pseudogenes). In this paper, the term “gene family” is used to describe a set of genes that are highly similar in sequence and are analyzed by Paraphase as a group.

Among the 160 gene families (Table S1), 149 have gene family members located on the same chromosome, with 16 in tandem (less than 10kb apart). To quantify the impact of sequence homology on read alignments, we examined the mapping qualities (MAPQs) in these regions in both short-read and long-read sequence data (Figure 1B). For short-read data, MAPQs are extremely low (76.4% have a median MAPQ<=20, and 98.8% have genomic segments with MAPQ<=20), indicating the difficulty of mapping short reads to these regions. Even for long-read data, 44.1% of the regions have a median MAPQ<=20 and 75.2% have genomic segments with MAPQ<=20. There are 25 (15.6%) gene families where the median MAPQ is 60 and there are no bases with MAPQ<=20 in the long-read data. These are either regions where the homology extends less than the HiFi read length of ~15-20 kb or regions included in Paraphase for fusion calling between less similar paralogs (see Methods). Paraphase analysis is still needed in these high MAPQ regions because: 1) reads with high MAPQ can be misaligned due to reference genome artifacts, common CNVs and high rates of gene conversion, 2) gene fusions are hard to detect because split alignments are unlikely to happen in regions of homology and 3) lower MAPQs are expected in data with shorter read length, such as in HiFi hybrid capture data.

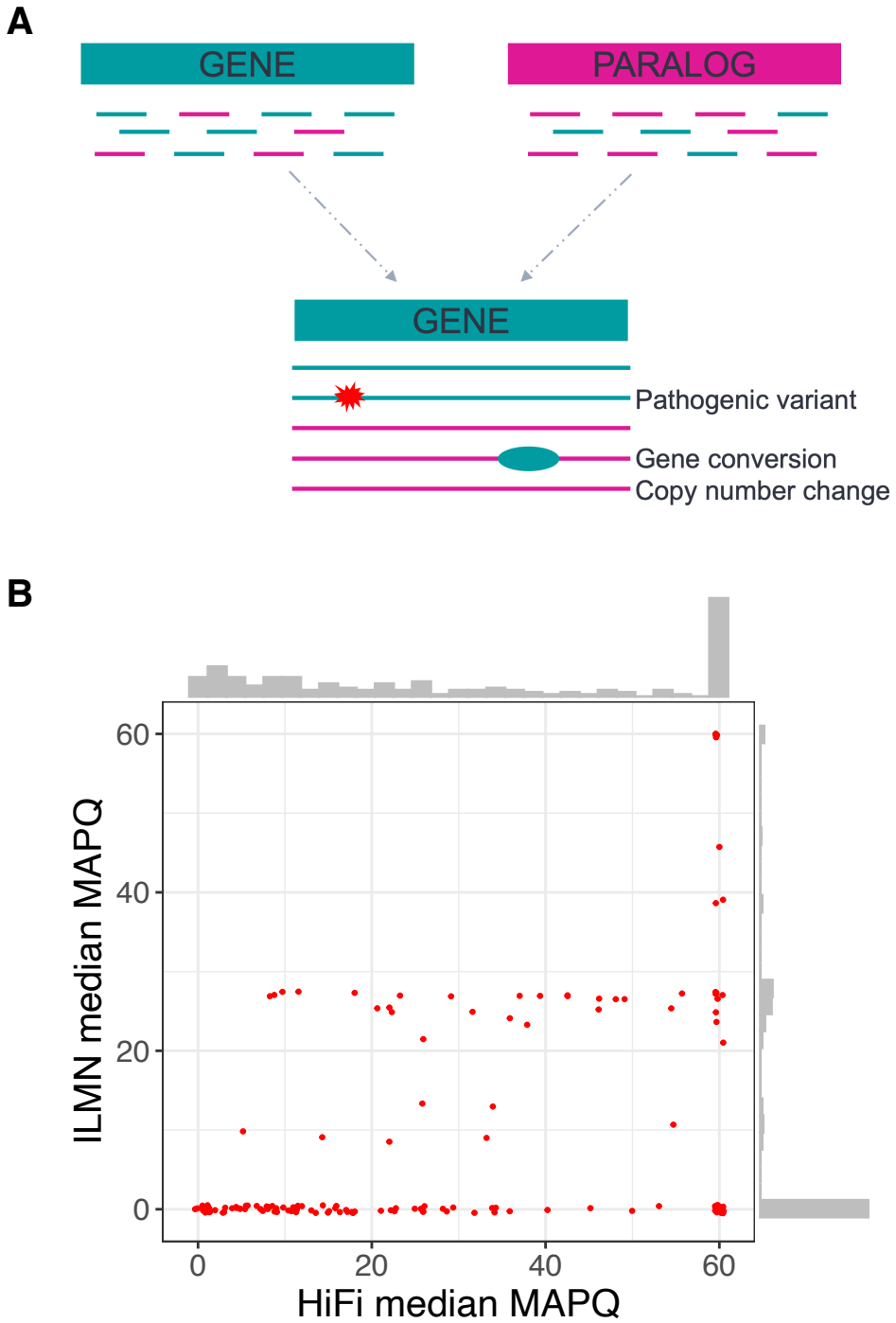

135

136 Figure 1. Paraphase design and the regions it analyzes.

137 **A.** Paraphase extracts reads that align to gene families, realigns to the archetype gene, and
138 phases reads into haplotypes. Variant calling is performed on each haplotype. **B**. Comparison of
139 median MAPQ between HiFi and Illumina WGS data in 160 groups of homologous regions
140 analyzed by Paraphase, highlighting mapping difficulty in these challenging regions for both
141 short and long reads.

Validation of Paraphase calls

We first validated Paraphase variant calls in 8 medically relevant genes in 21 disease or carrier samples using orthogonal methods such as MLPA and Sanger sequencing (Table 1 and Table S2, also see Methods). For this validation, Paraphase correctly identified all 30 of the clinical variants in these samples.

We also examined haplotypes called by Paraphase in 36 trios. Among 14,734 full-length haplotypes called in the probands (also requiring full-length haplotypes called in the two parents of each trio), 14,679 (99.6%) agreed exactly with one of the haplotypes observed in the parents. Upon examining the 55 inconsistent haplotypes, 43 (0.29%) are Paraphase errors (switch errors or extra or missing haplotypes), and the remaining 12 (0.081%) are true recombination or *de novo* events (See “Identification of *de novo* mutations and gene conversion” section).

Table 1. Paraphase calls in medically relevant genes validated by orthogonal methods

Gene	Variants	Number of alleles
CYP21A2	Gene deletion	1
	CYP21A1P-CYP21A2 fusion	1
	Pathogenic small variant	4
STRC	Gene deletion	3
	Pathogenic small variant	1
SMN1	0 copies of *SMN1* (Absence of c.840C)	2
PMS2	Hybrid *PMS2* with *PMS2CL* sequence	1
	Pathogenic SV	3
OPN1LW/OPN1MW	Pathogenic small variant	3
	Pathogenic CNV and pathogenic small variant	2
IKBKG	Pathogenic SV	1
NCF1	Gene deletion	4
	Pathogenic small variant	2
CFC1	Pathogenic small variant	2
Total		30

CN variability of gene families

We calculated the distribution of the total CN (defined by the number of unique haplotypes, adjusted by depth) of each gene family in 259 unrelated individuals across five ancestral populations. We assessed the variability of the total CN by the percentage of individuals having the mode CN. For this study, we say that a gene family has low CN variability if more than 90% of the individuals have the mode CN value. Conversely, a gene family is defined as having high CN variability if less than 90% of individuals have the mode CN value. Based on these definitions, 79 of the gene families have low CN variability and 81 have high CN variability (Figure 2A, Table S1). Additionally, 25.6% (41/160) of the gene families had significant (Chi-squared test, $p<0.05$, with Bonferroni correction) deviations between ancestral populations (Figure S1).

The CN variability can give us a general understanding of the population-level “accuracy” of the reference genome (in this case GRCh38). For example, an SD with two homologous regions like *SMN1*/*SMN2* would always have a CN of four in our analysis if the reference is correct and generalizes across the population. Likewise, a gene family where every individual has a CN of two in the population is likely a false SD in the reference. We identified 22 gene families where more than 95% of all individuals have a total CN of two (Table S3, Figure 2B). This suggests that duplications are rare in the population for these genes and these SDs could represent errors in the reference genome. Nineteen of these gene families overlap regions that were classified as false duplications in GRCh38 based on the CHM13 T2T assembly (Nurk et al. 2022). Conversely, three of these gene families (*DEFB109B, CNTNAP3/CNTNAP3C* and *POTED*; see Table S3) were not identified as false duplications in GRCh38 by the CHM13 T2T assembly. However, these three gene families are only present once in the CHM13 T2T assembly. Paraphase analysis of CHM13 data shows one haplotype in *DEFB109B* and *CNTNAP3/CNTNAP3C* but two haplotypes in *POTED*, where the additional haplotype could be due to mosaicism, as the coverage of this region is similar to the genome average (Figure S2).

Additionally, CHM13 has only one gene copy for the *CTAGE8/CTAGE9* family and the *OR2A1/OR2A42* family (Figure S2), resulting in missing genes (*CTAGE8* and *OR2A42*), which were attributed to false duplications in GRCh38 (Nurk et al. 2022). For another gene family, *RIMBP3/RIMBP3B/RIMBP3C*, CHM13 has two copies (Figure S2) and attributed the missing *RIMBP3* to a false duplication in GRCh38. All three of these gene families are truly CN variable regions in the population (distributions shown in Figure 2A) and thus not false duplications in GRCh38.

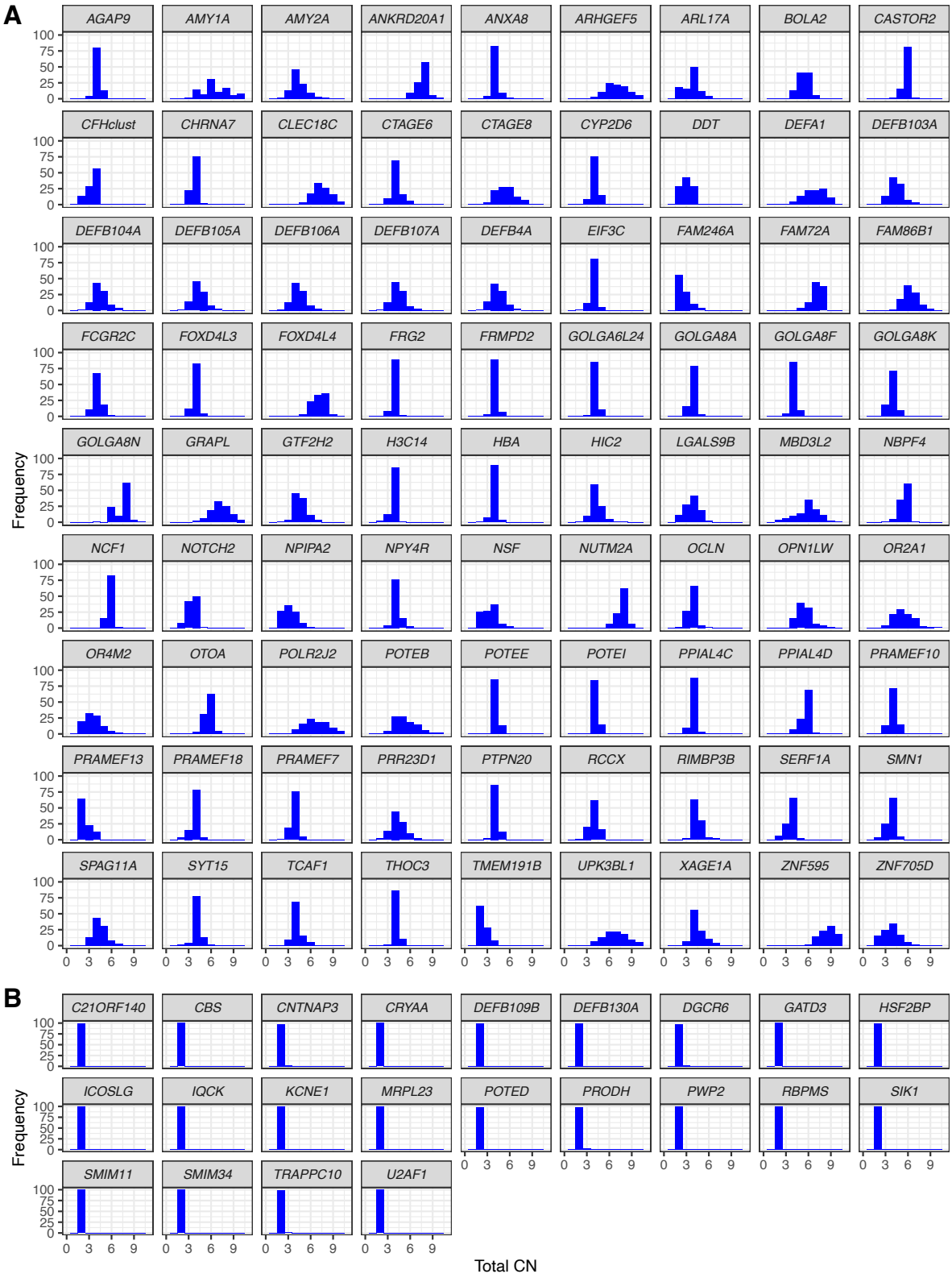
A
AGAP9
AMY1A
AMY2A
ANKRD20A1
ANXA8
ARHGEF5
ARL17A
BOLA2
CASTOR2
CFHclust
CHRNA7
CLEC18C
CTAGE6
CTAGE8
CYP2D6
DDT
DEFA1
DEFB103A
DEFB104A
DEFB105A
DEFB106A
DEFB107A
DEFB4A
EIF3C
FAM246A
FAM72A
FAM86B1
FCGR2C
FOXD4L3
FOXD4L4
FRG2
FRMPD2
GOLGA6L24
GOLGA8A
GOLGA8F
GOLGA8K
GOLGA8N
GRAPL
GTF2H2
H3C14
HBA
HIC2
LGALS9B
MBD3L2
NBPF4
NCF1
NOTCH2
NPIPA2
NPY4R
NSF
NUTM2A
OCLN
OPN1LW
OR2A1
OR4M2
OTOA
POLR2J2
POTEB
POTEE
POTEI
PPIAL4C
PPIAL4D
PRAMEF10
PRAMEF13
PRAMEF18
PRAMEF7
PRR23D1
PTPN20
RCCX
RIMBP3B
SERF1A
SMN1
SPAG11A
SYT15
TCAF1
THOC3
TMEM191B
UPK3BL1
XAGE1A
ZNF595
ZNF705D
B
C21ORF140
CBS
CNTNAP3
CRYAA
DEFB109B
DEFB130A
DGCR6
GATD3
HSF2BP
ICOSLG
IQCK
KCNE1
MRPL23
POTED
PRODH
PWP2
RBPMS
SIK1
SMIM11
SMIM34
TRAPPC10
U2AF1
Frequency
Total CN

193

Figure 2. Distribution of the total CN of each gene family across populations.

One archetype gene is selected to represent the name of each family. **A**. Gene families with high CN variability. For the two gene families (*OPN1LW* and *XAGE1A*) located on the X chromosome, only female samples are plotted. **B**. False duplication regions in GRCh38, where the majority of individuals have a total CN of two.

Gene families with exceptionally low within-family diversity

Paraphase identified 159,795 haplotypes from the 160 gene families in the 259 samples. Extensive gene conversion and unequal crossing over can result in highly similar gene copies that can no longer be separated into different genes based on sequence alone. For example, *SMN1* and *SMN2* are different in sequence in Exons 7-8, but are indistinguishable in Exons 1-6 indicating that gene conversion is much more common in Exons 1-6 than in Exons 7-8 (Chen et al. 2023). Thus, a principal component analysis (PCA) of variants in Exons 7-8 can differentiate *SMN1* haplotypes from *SMN2* haplotypes, but a PCA of variants in Exons 1-6 does not differentiate the genes (Figure S3).

To identify gene families with low within-family diversity, we developed a metric based on the heterozygosity (divergence) between individual haplotypes (see Methods). For example, in a gene family with a gene and a paralog, the gene will evolve independently from the paralog in the absence of gene conversion. This means that the heterozygosity will be lower between two copies of the gene (i.e. gene-gene heterozygosity) or two copies of the paralog in the absence of any selective pressures. Conversely, the gene-paralog heterozygosity will be significantly higher (Figure S4). Increasing rates of gene conversion and unequal crossing over will tend to make the gene more similar to the paralog and thus drive the gene-paralog heterozygosity down (Figure S4).

We identified 23 gene families (termed low-diversity gene families) where the within-family sequence divergence is comparable to the general allelic sequence divergence (See Methods). Among these, 4 are on chrY, 11 on chrX, and 8 on autosomes (Table 2). It is often not easy to assign haplotypes of a gene family to individual genes without prior knowledge of how genes and paralogs differ from each other. However, among the 23 low-diversity gene families, there are five where the phased haplotypes extend into non-homologous regions so that we can assign haplotypes to genes based on their flanking sequence: *AMY1A/AMY1B/AMY1C* (Figure 3A), *CTAG1A/CTAG1B*, *BOLA2/BOLA2B, SULT1A3/SULT1A4* and *SLX1A/SLX1B* (*BOLA2/BOLA2B, SULT1A3/SULT1A4, and SLX1A/SLX1B* are a group of three families in tandem and genotyped as one region by Paraphase). PCA of the haplotype sequences shows that haplotypes of the different genes of the same family are indistinguishable from each other (Figure 3B-D, also see Figure S5).

The 23 low-diversity gene families show two different patterns in their genomic structure, CN variability and evolutionary history (Table 2). Those on autosomes have high CN variability and many are human-specific duplications (See Discussion). Conversely, low-diversity gene families on sex chromosomes mostly have low CN variability, are arranged in palindrome structures and evolutionarily conserved, i.e. all gene family members are present in other primates where they are also in palindromes (Trombetta and Cruciani 2017; Jackson et al. 2021). Additionally, there are 3 palindromic families on chrX where the genes and paralogs are in tandem so we can identify copies on the same chromosome. In these 3 gene families, the gene copies in cis are more similar to each other than those in trans (Figure 3E), suggesting that gene conversion between arms of palindromes happens more frequently in cis (possibly through forming a hairpin structure) than in trans.

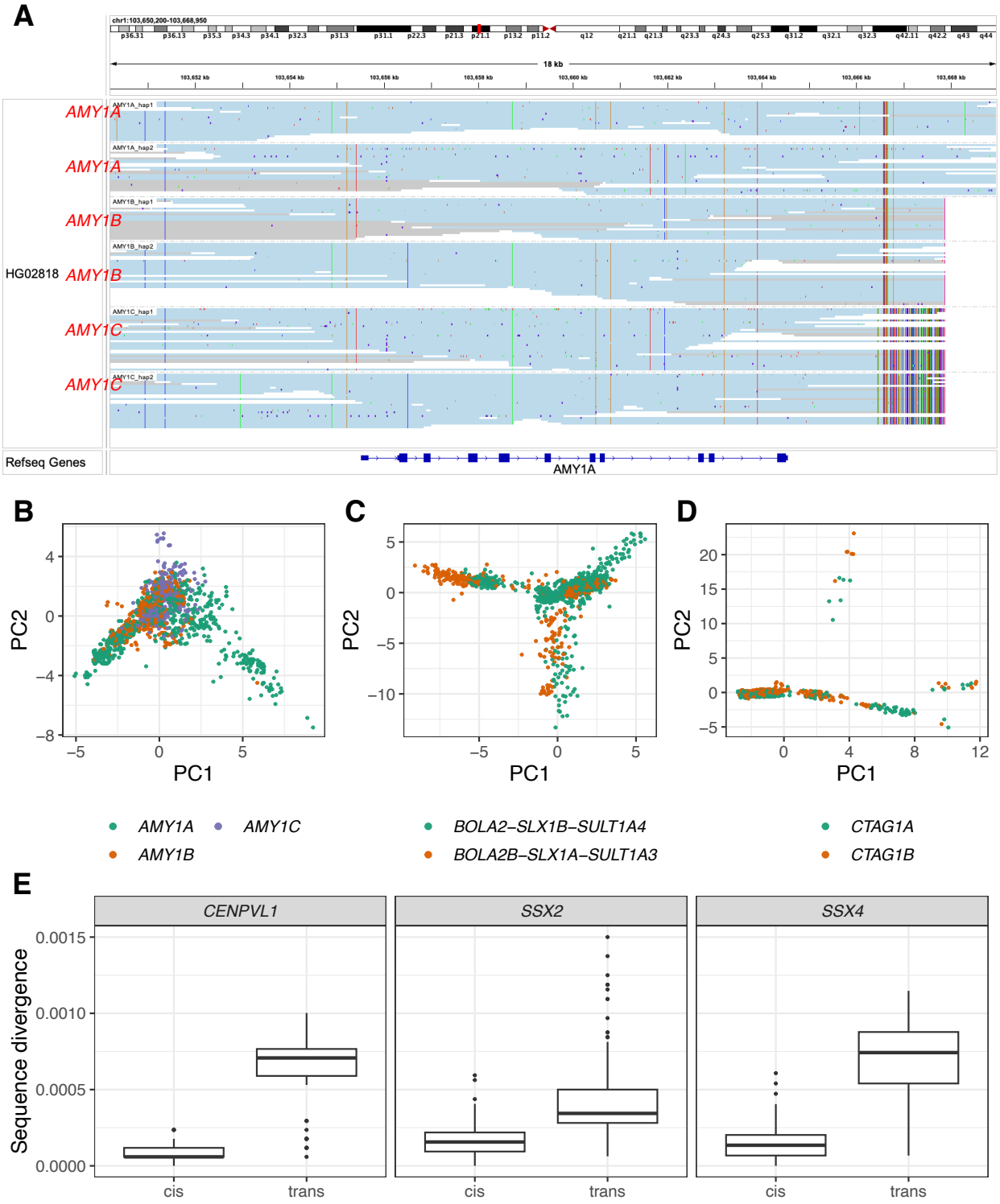
A
chr1:103,650,200-103,668,950
18 kb
AMY1A
AMY1A
AMY1B
HG02818
AMY1B
AMY1C
AMY1C
Refseq Genes
AMY1A
B
PC2
PC1
C
PC2
PC1
D
PC2
PC1
AMY1A
AMY1C
AMY1B
BOLA2–SLX1B–SULT1A4
BOLA2B–SLX1A–SULT1A3
CTAG1A
CTAG1B
E
CENPVL1
SSX2
SSX4
Sequence divergence
cis
trans

Figure 3. Gene families with low within-family diversity.

A. Haplotypes of the *AMY1* family in a sample, showing two copies each of *AMY1A*, *AMY1B* and *AMY1C.* Reads in blue are consistent with a single haplotype. Reads in gray are consistent with more than one possible haplotype, i.e. when two or more haplotypes are identical over a region. The ends of the haplotypes extend into downstream non-homologous regions so we can assign the haplotypes into the three genes. **B-D.** PCA of haplotype sequences of the *AMY1A/AMY1B/AMY1C* family (B), *BOLA2-SLX1B-SULT1A4/BOLA2B-SLX1A-SULT1A3* family (a group of three families in tandem and genotyped as one region by Paraphase) (C) and *CTAG1A/CTAG1B* family (D). Each dot represents a haplotype in the population. Colors represent different genes in a family as assigned according to the ending sequences of each haplotype (which extends into non-homologous regions). **E.** Sequence divergence between haplotypes in cis vs. trans in three palindromic gene families. One gene is selected to represent the name of each family (*CENPVL1*: *CENPVL1*/*CENPVL2*. *SSX2*: *SSX2*/*SSX2B*. *SSX4*: *SSX4*/*SSX4B*).

262 Table 2. Gene families with low within-family diversity.

	Gene families	Palindromic	High CN variability	Human-specific duplication
chrY	*BPY2/BPY2B/BPY2C*	x		
	CDY1/CDY1B	x		
	CDY2A/CDY2B	x		
	HSFY1/HSFY2	x		
chrX	*CENPVL1/CENPVL2*	x		
	CTAG1A/CTAG1B	x		
	CXorf49/CXorf49B	x		
	DMRTC1/DMRTC1B	x		
	FAM156A/FAM156B	x		
	MAGED4/MAGED4B	x		
	NXF2/NXF2B	x		
	SSX2/SSX2B	x		
	SSX4/SSX4B	x		
	TCP11X1/TCP11X2	x		
	XAGE1A/XAGE1B	x	x	
Autosomes	*SLX1A/SLX1B*		x	x
	BOLA2/BOLA2B		x	x
	SULT1A3/SULT1A4		x	x
	NPIPA2/NPIPA3		x	x
	AMY1A/AMY1B/AMY1C		x	x
	SERF1A/SERF1B		x	x
	EIF3C/EIF3CL		x	
	TRIM49D1/TRIM49D2	x		

263
264

Identification of *de novo* mutations and gene conversion

In 36 parent-offspring trios we identified 12 events (6 paternal and 6 maternal) where a haplotype in the proband is different from the corresponding haplotype in the parent (Figure S6-S16). Eleven of these are *de novo* events where the proband haplotype differs from the parent haplotype by one SNV. Among these, 7 are *de novo* SNVs and 4 are products of gene conversion. Among the gene conversion cases, 2 are non-allelic (an example is shown in Figure 4), 1 is allelic and 1 could be either allelic or non-allelic. Among the 11 *de novo* events, 4 are intergenic, 6 are in introns, and 1 is in an exon (synonymous). The remaining case of the 12 events is a hybrid haplotype between two haplotypes from the same parent, which could arise through equal or unequal crossing over (inconclusive without longer range phasing information in the parent due to the high copy number of the gene family) (Figure S16).

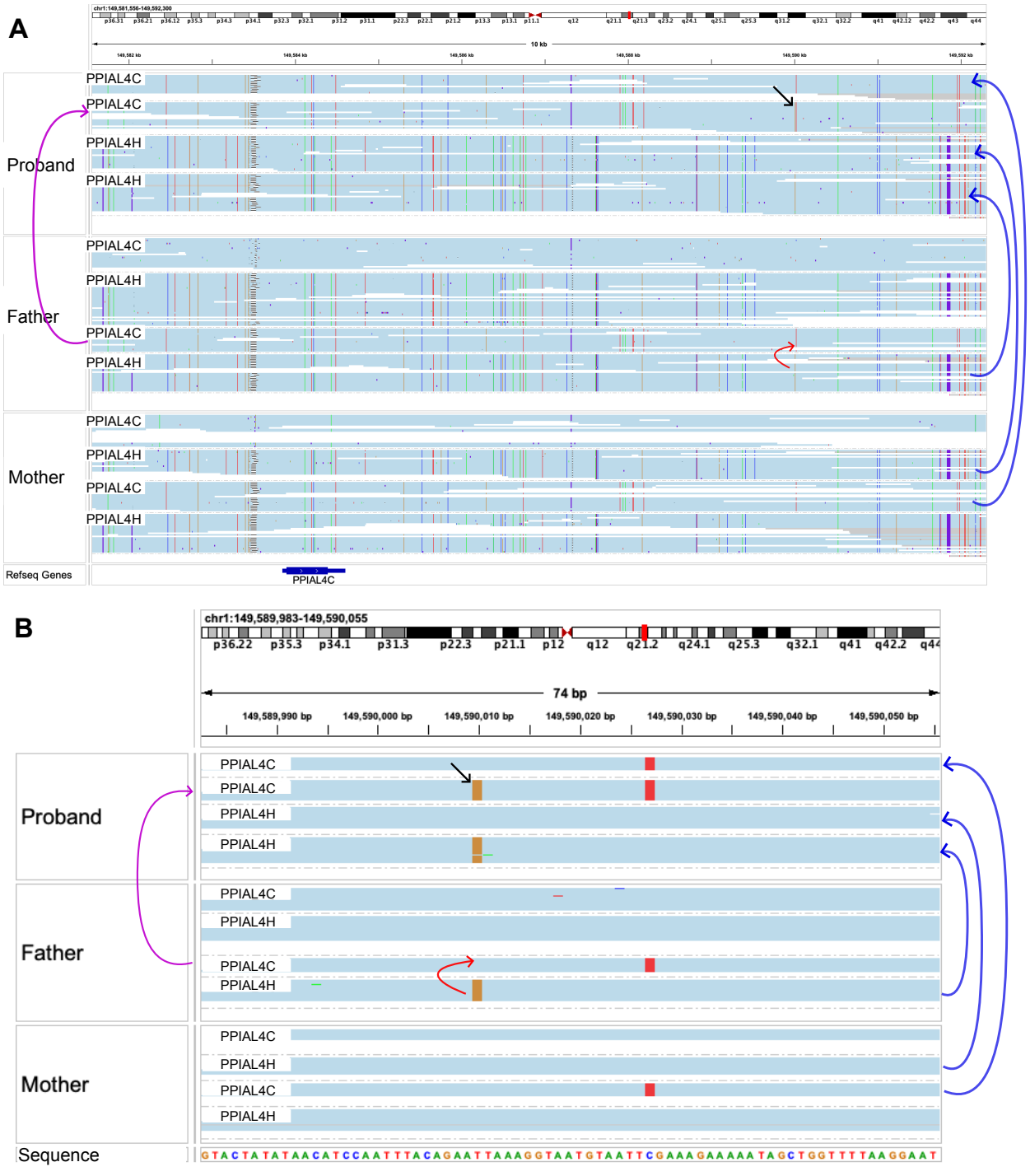

Figure 4. *De novo* non-allelic gene conversion in a trio.

A. The black arrow denotes the SNV created by non-allelic gene conversion on haplotype 2 of the proband. It is not present on the inherited haplotype, haplotype 3 in the father. Instead, it is present on haplotype 4 of the father, which belongs to the other gene in the family. The magenta arrow on the left indicates the inheritance of the converted haplotype. The blue arrows on the right indicate the inheritance of the other haplotypes. The red arrow shows the direction of the gene conversion. **B.** Close view of the converted variant.

Resolving medically relevant homologous genes

As a demonstration of how Paraphase can be used to study gene families in the population, we examined variant and haplotype frequencies across populations in three known medically relevant gene families, *CYP21A2/CYP21A1P*, *PMS2/PMS2CL* and *OPN1LW*/*OPN1MW*.

Variants in *CYP21A2* cause 21-Hydroxylase-Deficient Congenital Adrenal Hyperplasia (21-OHD CAH) (Merke and Auchus 2020). *CYP21A2* resides in a 30-kb tandem repeat called the RCCX module that includes its pseudogene, *CYP21A1P*, together with two other pairs of paralogs, *C4A/C4B* and *TNXB/TNXA* (Pignatelli et al. 2019; Merke and Auchus 2020) (Figure 5A). This region is susceptible to gene conversion (Merke and Auchus 2020), as well as deletions and duplications of the RCCX module resulting in CN changes and disease-causing hybrid genes between *CYP21A2* and *CYP21A1P*. The total CN of RCCX is highly variable across populations (Figure 5B) with 38.2% of individuals having a CNV. Figure 5A shows examples of samples with various CNs. In addition, we identified a duplication allele (Figure 5A, bottom panel) that carries a copy of *CYP21A1P*, a copy of *CYP21A2* with a stop-gain variant Q319X, and a second functional copy of *CYP21A2*. This allele is found at 1-2% frequency in the populations (Table S4) and, without phasing the full region, could be misidentified as a pathogenic allele due to the presence of Q319X. Researchers have previously found that individuals with Q319X frequently have a duplication of *CYP21A2*, which complicates *CYP21A2* testing (Lekarev et al. 2013). Paraphase can distinguish a *CYP21A2*+*CYP21A2*(Q319X) allele vs. a *CYP21A2*(Q319X) allele.

Pathogenic variants in *PMS2* cause Lynch syndrome (ten Broeke et al. 2018). In its last few exons (Exons 12-15), *PMS2* has high sequence similarity to its pseudogene *PMS2CL*, and gene conversion and unequal crossing overs are known to promote sequence exchange between the two genes (Hayward et al. 2007; van der Klift et al. 2010; Ganster et al. 2010). In Exon 15, the sequences of *PMS2* and *PMS2CL* are indistinguishable from each other, lacking any differentiating variants (Figure 5C, also see PCA in Figure S17). For example, a commonly considered *PMS2CL*-specific variant (Wernstedt et al. 2012), NM_000535.7:c.*92dup, is in 72.8% of *PMS2CL* alleles and 31.1% of *PMS2* alleles. We found that gene conversion happens between *PMS2* and *PMS2CL* occasionally in Exon 12 and frequently in Exons 13-14 (See Methods and Figure 5C-D). Interestingly, our analysis shows more evidence of gene conversion in individuals of African ancestry, and more than 75% of African *PMS2*/*PMS2CL* alleles are partially or fully converted (Figure 5D).

OPN1LW and its paralog *OPN1MW* are responsible for red-green color vision deficiencies and other vision conditions such as blue cone monochromacy (BCM) (Neitz and Neitz 2011). The region is arranged in a gene array and only the first two genes in the array are expressed (Neitz and Neitz 2011). Paraphase identifies all copies of the repeat, assigns genes to *OPN1LW* or *OPN1MW*, and identifies the first two copies in the array on each chromosome. Figure 5E shows alleles with one copy each of *OPN1LW* and *OPN1MW* (top panel), as well as alleles that only have *OPN1LW* (middle panel) or *OPN1MW* (bottom panel) in the first two copies of the array. The total CN of this array is highly variable among populations (Figure 5F). Allele frequencies are summarized in Table S5, including alleles that cause color vision deficiencies.

328 In addition to the three gene families described above, we also summarized population results
329 for other medically relevant genes, including *SMN1/SMN2* (spinal muscular atrophy (Lunn and
330 Wang 2008), Figure S18), *STRC* (hereditary hearing loss and deafness (Yokota et al. 2019),
331 Figure S19), *HBA1/HBA2* (Alpha thalassemia (Farashi and Harteveld 2018), Table S6), *IKBKG*
332 (Incontinentia Pigmenti (Cammarata-Scalisi et al. 2019), Table S7), the *CFH* gene cluster
333 (*CFH/CFHR1/CFHR2/CFHR3/CFHR4*) (atypical hemolytic uremic syndrome (Zipfel et al. 2007)
334 and age-related macular degeneration (Klein et al. 2005; Hughes et al. 2006), Table S8) and
335 *GBA* (Gaucher and Parkinson's disease (Hruska et al. 2008; Sidransky et al. 2009), Table S9).
336 Together, we identified medically relevant variants in these 9 gene families in 75%, 49.6%,
337 45.8%, 52.2% and 17.4% of individuals of African, European, Admixed American, South Asian
338 and East Asian ancestries, respectively.

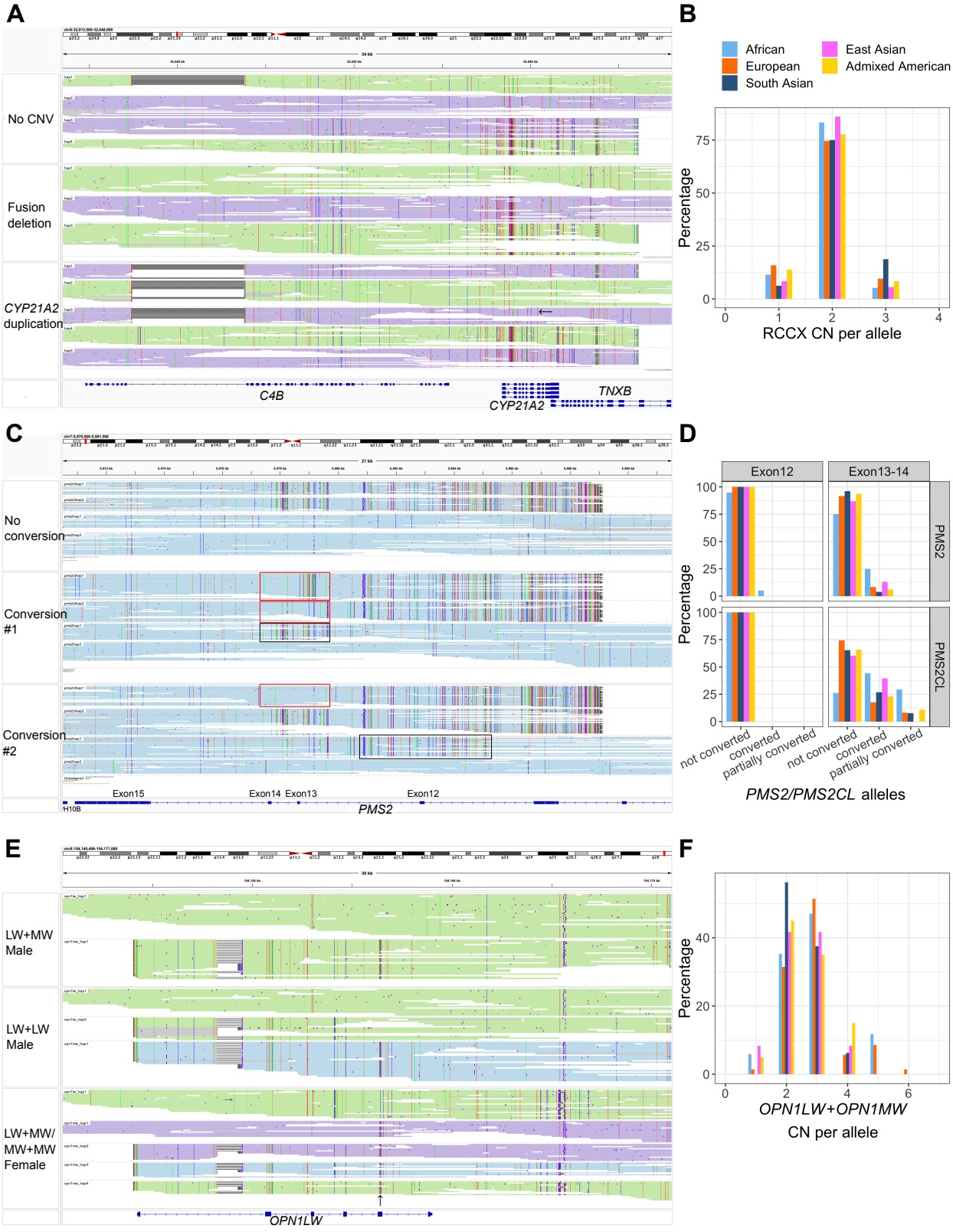
A
No CNV
Fusion deletion
CYP21A2 duplication
C4B
CYP21A2
TNXB
B
African
European
South Asian
East Asian
Admixed American
Percentage
RCCX CN per allele
C
No conversion
Conversion #1
Conversion #2
Exon15
Exon14
Exon13
Exon12
PMS2
D
Exon12
Exon13-14
PMS2
PMS2CL
Percentage
not converted
converted
partially converted
PMS2/PMS2CL alleles
E
LW+MW Male
LW+LW Male
LW+MW/ MW+MW Female
OPN1LW
F
Percentage
OPN1LW+OPN1MW
CN per allele

339

Figure 5. Population results in *CYP21A2*, *PMS2* and *OPN1LW/OPN1MW*.

A. Paraphase resolved haplotypes in the RCCX module, realigned to the RCCX copy that encodes *CYP21A2*. Haplotypes of the same color (purple or green) are from the same allele. Longer haplotypes represent the last RCCX copies in the array on each allele, and shorter haplotypes represent remaining copies. Three examples are shown, including a sample with no CNV (top), a sample with fusion deletion (*CYP21A1P-CYP21A2* fusion, middle, purple allele) and a sample with RCCX duplication (bottom). The bottom sample carries an allele (purple) with a wild-type copy of *CYP21A2* and another copy of *CYP21A2* harboring a pathogenic variant Q319X (black arrow). **B.** Frequency of the total RCCX CN per allele across populations. **C.** Paraphase resolved haplotypes in *PMS2*/*PMS2CL*, realigned to *PMS2*. Exon numbers are labeled with respect to *PMS2*. Longer haplotypes represent *PMS2* copies and shorter ones represent *PMS2CL* copies. Three examples are shown, including a sample with no gene conversion and two samples carrying alleles converted in Exon12 or Exon13-14 (conversions in *PMS2* shown in black boxes and conversions in *PMS2CL* shown in red boxes). **D.** Frequency of gene conversions between *PMS2* and *PMS2CL* across populations in Exon12 and Exon13-14. **E.** Paraphase resolved haplotypes in *OPN1LW*/*OPN1MW*, realigned to *OPN1LW*. Haplotypes of the same color (purple or green) are from the same allele. Longer haplotypes represent the first copies of the repeat in the array on each allele, and shorter haplotypes represent remaining copies. The blue color indicates gene copies beyond the second copy in the array, i.e. not expressed. *OPN1LW* and *OPN1MW* are assigned based on variants in Exon5 (black arrow). Three examples are shown, including a normal allele with a copy of *OPN1LW* followed by a copy of *OPN1MW* (top), an allele (*deutan*) with a copy of *OPN1LW* followed by a copy of *OPN1LW* (middle, the third unexpressed copy marked in blue), and a female sample where one normal allele has a copy of *OPN1LW* followed by a copy of *OPN1MW*, and the other allele (*protan*) has a copy of *OPN1MW* followed by a copy of *OPN1MW* (bottom, the third unexpressed copy marked in blue). **F.** Distribution of the summed CN of *OPN1LW* and *OPN1MW* per allele across populations.

Discussion

In this paper, we applied Paraphase to 160 segmental duplication regions where large (>10kb) regions of high (>99%) sequence similarity exist between genes and their paralogs. By phasing reads from the same gene family together, Paraphase can recover misaligned reads and correctly resolve genes together with their highly similar paralogs/pseudogenes. This method enables high-throughput CN detection and genotyping of SD-encoded genes with only HiFi data at standard WGS depth (30X).

An important benefit of the gene-family-centered approach is that it is not influenced by the CN difference between an individual and the reference, and it can work even when the CN of a gene family does not agree with the reference genome in most individuals of the population, such as in the case of false segmental duplications in GRCh38. In addition, by calling variants against the same reference gene within a gene family, Paraphase outputs gene copies that can be easily compared against each other, allowing us to perform within-family divergence analysis, as well as to detect de novo mutations including gene conversion events between paralogs. Our analysis of 36 trios identified 7 *de novo* SNVs and 4 *de novo* gene conversion events, demonstrating the power of long-read sequencing in detecting de novo variations (Noyes et al. 2022; Kucuk et al. 2023), particularly in previously inaccessible regions of the genome.

Among regions analyzed by Paraphase, we observed that gene families on sex chromosomes are more CN invariable (93.1% of gene families on sex chromosomes have low CN variability vs. 39.7% on autosomes) and have drastically lower within-family diversity (median pairwise haplotype divergence 0.00033 on sex chromosomes vs. 0.00187 on autosomes, p-value 4.179e-11). This could be related to the fact that most gene families on sex chromosomes are arranged in palindrome structures (86.2% vs. 16.8% on autosomes). Unequal crossing overs between arms of a palindrome result in inversions and do not change the copy number. Arm-to-arm gene conversion is known to occur frequently to prevent sex chromosomes from accumulating deleterious mutations in the absence of homologous chromosomes (Swanepoel et al. 2020; Jackson et al. 2021), and could contribute to the low within-family diversity.

We identified 23 gene families with extremely low within-family diversity (Table 2), where extensive gene conversion and/or unequal crossing over have resulted in paralogs that are as similar as alleles from the same gene. Consistent with most other families on sex chromosomes, the low-diversity gene families on sex chromosomes are all arranged in palindromes and mostly have low CN variability. For these gene families, both the genes and the palindrome structure are evolutionarily conserved in other primates. The low-diversity gene families on autosomes, however, are not arranged in palindrome structure and mostly have high CN variability. Interestingly, many of these gene families are duplicated exclusively in the human lineage, with positive selection detected, e.g. *AMY1A*/*AMY1B*/*AMY1C* (Perry et al. 2007), *BOLA2/BOLA2B* (Nuttle et al. 2016; Giannuzzi et al. 2019) and *SULT1A3/SULT1A4* (Butcher et al. 2018). It is possible that extensive gene conversion and unequal crossing over happens between members of these families to prevent the newly duplicated genes from

412 diverging to maintain an elevated gene dosage in humans. For example, the CN of the salivary
413 amylase gene (*AMY1A*/*AMY1B*/*AMY1C*, Figure 3A-B) is variable between populations (Figure
414 S1) and is correlated with salivary amylase level (Perry et al. 2007). *AMY1* is under positive
415 selection so that populations with high-starch diets have more copies of *AMY1*, which improves
416 the digestion of starchy foods (Perry et al. 2007). Beyond gene families with low within-family
417 diversity throughout the entire gene body, one future direction is to extend this analysis to
418 identify local low-diversity regions resulting from gene conversions, such as the gene
419 conversion found in Exons 1-6 of *SMN1/SMN2* (Figure S3), and Exon 15 of *PMS2* (Figure 5C,
420 Figure S17).
421
422 The SD-encoded genes presented in this paper were previously inaccessible to population-wide
423 genomic analyses and hence are largely missing from variant annotation databases such as
424 gnomAD (Karczewski et al. 2020), creating hurdles in variant interpretation. Here we provide a
425 database (https://zenodo.org/doi/10.5281/zenodo.10909886) of variant allele frequencies
426 collected from the population samples used in this paper. This annotation resource can be
427 further expanded as more HiFi data are generated and analyzed with Paraphase.
428
429 One limitation of Paraphase is that currently it focuses on gene families with <10 copies in an
430 individual and does not include other highly similar genes with even higher CNs. This excludes
431 79 genes that fall into SDs in our analysis. Nevertheless, Paraphase can be customized to
432 analyze user-specific regions, allowing new targets to be added in the future.
433
434 Paraphase, combined with HiFi long reads, provides a single framework for resolving
435 paralogous genes. In medically important genes challenged by pseudogenes or paralogs,
436 Paraphase helps enable more accurate testing to detect pathogenic variants, thus bringing us
437 one step closer to consolidating the numerous currently offered genetic tests into a single test.
438 Furthermore, in previously inaccessible and less studied genes, population-wide sequencing
439 based analysis with Paraphase will facilitate the discovery of novel gene-disease associations.

440

Methods

Paraphase: HiFi-based caller for highly similar paralogous genes

Paraphase is designed to work with both PacBio HiFi WGS and target enrichment data. Paraphase resolves a group of highly similar genes by extracting HiFi reads aligned to any member of the family, realigning them to the archetype gene, and phasing them into haplotypes, followed by variant calling on each haplotype (Chen et al. 2023) (Figure 1A). Realigning all reads from all genes of the same gene family to one gene bypasses the error-prone process of aligning reads to multiple similar regions. This framework enables all copies of the gene family, including genes and their paralogs or pseudogenes, to be examined for variants and annotated for functional status.

When two homologous regions are in tandem, Paraphase uses read-based phasing to further phase gene haplotypes into alleles, i.e. gene copies on the same chromosome, by grouping haplotypes that have an overlapping set of supporting reads. For example, for the RCCX module demonstrated in Figure 5A, reads are grouped by the haplotypes they originate from and haplotypes of the same color (green or purple) represent those from the same allele.

Gene fusions between paralogs are called by detecting haplotypes whose flanking regions (upstream and downstream of the homologous region) are consistent with two different genes. Fusion breakpoints are called by detecting a switch in bases at the paralogous sequence variant (PSV) sites.

Within Paraphase, there are a few gene-specific callers for medically relevant genes. These callers use gene-specific information during analysis, for example, known sequence differences between genes and paralogs/pseudogenes. In addition, these callers produce gene-specific output information such as hybrid gene structures and known pathogenic variants, including large difficult-to-call structural variants.

Genome-wide identification of highly similar genes for analysis by Paraphase

We extracted 19,394 Ensembl protein coding genes (>20 kb sequences centered on each gene, adding flanking sequences for shorter genes) and aligned them against GRCh38 (ALT contigs excluded, pseudoautosomal regions (PARs) masked). We selected genes that had alignment matches >10 kb in length and >99% in sequence similarity as candidate gene families. The majority of genes have zero paralogs, and the remaining ones vary in the number of paralogs (Figure S20). Among genes with three or fewer paralogs, which represent the majority of genes with paralogs, we incorporated into Paraphase 155 groups of regions. In addition, we included genes impacted by shorter homology or lower sequence similarity, where gene fusions are highly medically relevant yet difficult to call by conventional SV callers due to homology, including *HBA1/HBA2* (Alpha thalassemia), *GBA1/GBAP1* (Gaucher and Parkinson's disease), *CYP2D6/CYP2D7* (pharmacogenomics), *CYP11B1/CYP11B2* (Glucocorticoid-remediable

481 aldosteronism) and *CFH/CFHR1/CFHR2/CFHR3/CFHR4* (atypical hemolytic uremic syndrome
482 and age-related macular degeneration). In total, Paraphase analyzes 160 groups of regions
483 (Table S1), which encode 316 genes in total (pseudogenes are not included).

484 MAPQ distributions

485 We selected 20 samples from five ancestral populations with both Illumina (data downloaded
486 from the 1000 Genomes Project (The 1000 Genomes Project Consortium 2015)) and HiFi WGS
487 data available to assess alignment MAPQs. For each gene family of interest, we calculated the
488 median values across the MAPQs of all reads aligned to the homology region in any gene of the
489 gene family.

490 Validation

491 Validation samples were collected from 21 clinical samples (disease or carrier samples) with 30
492 pathogenic variants in 8 disease-causing genes that were previously validated by orthogonal
493 methods, such as MLPA and Sanger sequencing (Table 1 and Table S2). In addition, we used
494 36 trios to examine the consistency of haplotypes called in probands vs. parents. Among the 36
495 trio, 8 were collected from Radboud University Medical Center, 10 were from the 100,000
496 Genomes Project and 18 were from Genomics Research to Elucidate the Genetics of Rare
497 Diseases (GREGoR) Consortium.

498 Population samples

499 For frequency calculations, we used 259 unrelated individuals from five ancestral populations
500 (113 Europeans, 52 Africans, 48 Admixed Americans, 23 South Asians and 23 East Asians),
501 collected from the Human Pangenome Reference Consortium (HPRC) (Wang et al. 2022; Liao
502 et al. 2023), the 100,000 Genomes Project, Radboud University Medical Center, Genomics
503 Research to Elucidate the Genetics of Rare Diseases (GREGoR) Consortium, and Genomic
504 Answers for Kids (GA4K) at Children's Mercy Kansas City.
505

506 Gene families with low within-family diversity

507 We searched for gene families within which the haplotype diversity is comparable to the general
508 sequence diversity between alleles of the same gene. To profile the average allelic sequence
509 divergence, we used Paraphase to phase haplotypes sequences for 600 randomly selected
510 genes (400 on autosomes and 200 on chrX) that fall outside of SDs, i.e. each individual is
511 expected to have two copies of a gene when there is no CNV, in the same set of 259
512 individuals. Focusing only on SNVs in non-homopolymer regions, 90% of the sequence
513 divergence among haplotypes were lower than 0.00156 for autosomal genes (Figure S21), and
514 for chrX genes, 90% of the sequence divergence among haplotypes were lower than 0.00101
515 (Figure S21), consistent with a lower mutation rate on chrX (Hodgkinson and Eyre-Walker
516 2011). To obtain candidate gene families where the within-family sequence divergence is as low
517 as the general allelic diversity, we required that 90% of the sequence divergence among

518 haplotypes of the same gene family to be lower than 0.00156 and 0.00101 for autosomal and
519 sex chromosome gene families, respectively. For both randomly selected genes and Paraphase
520 gene families, only haplotypes from the same ancestral populations were compared for pairwise
521 divergence calculation. Between a pair of haplotypes, sequence divergence was calculated by
522 dividing the number of base differences by the length of the region. For gene families reported
523 in Table 2, we further filtered out gene families where the homology does not span the entire
524 gene, i.e. partial paralogs. Principal component analysis (PCA) within a gene family was
525 conducted on SNV sites identified across all haplotypes of the gene family using the prcomp
526 function in R.

527 *PMS2* gene conversion calling

528 *PMS2* and *PMS2CL* haplotype sequences in Exon 12 region (chr7:5,981,000-5,985,000,
529 GRCh38) and Exons 13-14 region (chr7:5,977,000-5,980,000) are separated into two main
530 groups (*PMS2*-like and *PMS2CL*-like) based on the PCA (Figure S17). Variants (called against
531 the *PMS2* reference sequence) that are present in >95% of the *PMS2CL*-like group and <5% of
532 the *PMS2*-like group are selected as signature sites for calling gene conversion. Gene
533 conversion is called when a *PMS2CL* haplotype has <20% of the signature variants or when a
534 *PMS2* haplotype has >80% of the signature variants. A partial conversion in Exons 13-14 is a
535 special haplotype common in the population, called based on a predefined subset of the
536 signature variants (Figure 5C, middle panel, first haplotype).

537

Data access

Paraphase can be downloaded from https://github.com/PacificBiosciences/paraphase
HPRC HiFi data can be downloaded from https://github.com/orgs/human-pangenomics/repositories

Acknowledgements

We thank John Belmont for his valuable comments for the manuscript. We acknowledge colleagues from the diagnostic division of the Human Genetics Department from Radboudumc (Genome Diagnostics Nijmegen) and the Radboud Genomics Technology Center for their technical assistance and the library preparation and sequencing of all samples provided from Radboudumc, in particular Ronny Derks, Amber den Ouden, Janneke Weiss, and Lonneke Haer-Wigman. We thank the Human Pangenome Reference Center (HPRC) for generating and releasing the HiFi WGS data. We thank the Genomic Answers for Kids (GA4K) program at Children's Mercy Kansas City for generating the GA4K HiFi sequencing data. This research was made possible through access to the 100,000 Genomes Project data in the National Genomic Research Library, which is managed by Genomics England Limited (a wholly owned company of the Department of Health and Social Care). The National Genomic Research Library holds data provided by patients and collected by the NHS as part of their care and data collected as part of their participation in research. The National Genomic Research Library is funded by the National Institute for Health Research and NHS England. The Wellcome Trust, Cancer Research UK and the Medical Research Council have also funded research infrastructure.

Declaration of interest

X.C., D.B., E.D. and M.A.E. are employees of PacBio. J.M.D., J.N., A.S.B., R.B., K.S.H., L.L., P.K. and S.N. are employees of GeneDx.

References

Bailey JA, Yavor AM, Massa HF, Trask BJ, Eichler EE. 2001. Segmental Duplications: Organization and Impact Within the Current Human Genome Project Assembly. *Genome Res* **11**: 1005–1017.

Butcher NJ, Horne MK, Mellick GD, Fowler CJ, Masters CL, AIBL research group, Minchin RF. 2018. Sulfotransferase 1A3/4 copy number variation is associated with neurodegenerative disease. *Pharmacogenomics J* **18**: 209–214.

Bycroft C, Freeman C, Petkova D, Band G, Elliott LT, Sharp K, Motyer A, Vukcevic D, Delaneau O, O'Connell J, et al. 2018. The UK Biobank resource with deep phenotyping and genomic data. *Nature* **562**: 203–209.

Cammarata-Scalisi F, Fusco F, Ursini MV. 2019. Incontinentia Pigmenti. *Actas Dermosifiliogr* **110**: 273–278.

Chen J-M, Cooper DN, Chuzhanova N, Férec C, Patrinos GP. 2007. Gene conversion: mechanisms, evolution and human disease. *Nat Rev Genet* **8**: 762–775.

Chen X, Harting J, Farrow E, Thiffault I, Kasperaviciute D, Hoischen A, Gilissen C, Pastinen T, Eberle MA. 2023. Comprehensive SMN1 and SMN2 profiling for spinal muscular atrophy analysis using long-read PacBio HiFi sequencing. *Am J Hum Genet* **110**: 240–250.

Ebbert MTW, Jensen TD, Jansen-West K, Sens JP, Reddy JS, Ridge PG, Kauwe JSK, Belzil V, Pregent L, Carrasquillo MM, et al. 2019. Systematic analysis of dark and camouflaged genes reveals disease-relevant genes hiding in plain sight. *Genome Biol* **20**: 97.

Farashi S, Harteveld CL. 2018. Molecular basis of α-thalassemia. *Blood Cells Mol Dis* **70**: 43–53.

Ganster C, Wernstedt A, Kehrer-Sawatzki H, Messiaen L, Schmidt K, Rahner N, Heinimann K, Fonatsch C, Zschocke J, Wimmer K. 2010. Functional PMS2 hybrid alleles containing a pseudogene-specific missense variant trace back to a single ancient intrachromosomal recombination event. *Hum Mutat* **31**: 552–560.

Gao Y, Yang X, Chen H, Tan X, Yang Z, Deng L, Wang B, Kong S, Li S, Cui Y, et al. 2023. A pangenome reference of 36 Chinese populations. *Nature* **619**: 112–121.

Giannuzzi G, Schmidt PJ, Porcu E, Willemin G, Munson KM, Nuttle X, Earl R, Chrast J, Hoekzema K, Risso D, et al. 2019. The Human-Specific BOLA2 Duplication Modifies Iron Homeostasis and Anemia Predisposition in Chromosome 16p11.2 Autism Individuals. *Am J Hum Genet* **105**: 947–958.

Haer-Wigman L, den Ouden A, van Genderen MM, Kroes HY, Verheij J, Smailhodzic D, Hoekstra AS, Vijzelaar R, Blom J, Derks R, et al. 2022. Diagnostic analysis of the highly complex OPN1LW/OPN1MW gene cluster using long-read sequencing and MLPA. *Npj Genomic Med* **7**: 1–10.

Handsaker RE, Van Doren V, Berman JR, Genovese G, Kashin S, Boettger LM, McCarroll SA. 2015. Large multiallelic copy number variations in humans. *Nat Genet* **47**: 296–303.

Hayward BE, De Vos M, Valleley EMA, Charlton RS, Taylor GR, Sheridan E, Bonthron DT. 2007. Extensive gene conversion at the PMS2 DNA mismatch repair locus. *Hum Mutat* **28**: 424–430.

Hodgkinson A, Eyre-Walker A. 2011. Variation in the mutation rate across mammalian genomes. *Nat Rev Genet* **12**: 756–766.

Hruska KS, LaMarca ME, Scott CR, Sidransky E. 2008. Gaucher disease: mutation and polymorphism spectrum in the glucocerebrosidase gene (GBA). *Hum Mutat* **29**: 567–583.

Hughes AE, Orr N, Esfandiary H, Diaz-Torres M, Goodship T, Chakravarthy U. 2006. A common CFH haplotype, with deletion of CFHR1 and CFHR3, is associated with lower risk of age-related macular degeneration. *Nat Genet* **38**: 1173–1177.

614 Jackson EK, Bellott DW, Cho T-J, Skaletsky H, Hughes JF, Pyntikova T, Page DC. 2021. Large
615 palindromes on the primate X Chromosome are preserved by natural selection. *Genome*
616 *Res* **31**: 1337–1352.
617 Karczewski KJ, Francioli LC, Tiao G, Cummings BB, Alföldi J, Wang Q, Collins RL, Laricchia
618 KM, Ganna A, Birnbaum DP, et al. 2020. The mutational constraint spectrum quantified
619 from variation in 141,456 humans. *Nature* **581**: 434–443.
620 Klein RJ, Zeiss C, Chew EY, Tsai J-Y, Sackler RS, Haynes C, Henning AK, SanGiovanni JP,
621 Mane SM, Mayne ST, et al. 2005. Complement Factor H Polymorphism in Age-Related
622 Macular Degeneration. *Science* **308**: 385.
623 Kucuk E, van der Sanden BPGH, O'Gorman L, Kwint M, Derks R, Wenger AM, Lambert C,
624 Chakraborty S, Baybayan P, Rowell WJ, et al. 2023. Comprehensive de novo mutation
625 discovery with HiFi long-read sequencing. *Genome Med* **15**: 34.
626 Lekarev O, Tafuri K, Lane AH, Zhu G, Nakamoto JM, Buller-Burckle AM, Wilson TA, New MI.
627 2013. Erroneous prenatal diagnosis of congenital adrenal hyperplasia owing to a
628 duplication of the CYP21A2 gene. *J Perinatol Off J Calif Perinat Assoc* **33**: 76–78.
629 Liao W-W, Asri M, Ebler J, Doerr D, Haukness M, Hickey G, Lu S, Lucas JK, Monlong J, Abel
630 HJ, et al. 2023. A draft human pangenome reference. *Nature* **617**: 312–324.
631 Lunn MR, Wang CH. 2008. Spinal muscular atrophy. *Lancet Lond Engl* **371**: 2120–2133.
632 Mandelker D, Schmidt RJ, Ankala A, McDonald Gibson K, Bowser M, Sharma H, Duffy E,
633 Hegde M, Santani A, Lebo M, et al. 2016. Navigating highly homologous genes in a
634 molecular diagnostic setting: a resource for clinical next-generation sequencing. *Genet*
635 *Med Off J Am Coll Med Genet* **18**: 1282–1289.
636 Merke DP, Auchus RJ. 2020. Congenital Adrenal Hyperplasia Due to 21-Hydroxylase
637 Deficiency. *N Engl J Med* **383**: 1248–1261.
638 Neitz J, Neitz M. 2011. The genetics of normal and defective color vision. *Vision Res* **51**: 633–
639 651.
640 Neitz M, Neitz J. 2021. Intermixing the OPN1LW and OPN1MW Genes Disrupts the Exonic
641 Splicing Code Causing an Array of Vision Disorders. *Genes* **12**: 1180.
642 Noyes MD, Harvey WT, Porubsky D, Sulovari A, Li R, Rose NR, Audano PA, Munson KM,
643 Lewis AP, Hoekzema K, et al. 2022. Familial long-read sequencing increases yield of de
644 novo mutations. *Am J Hum Genet* **109**: 631–646.
645 Nurk S, Koren S, Rhie A, Rautiainen M, Bzikadze AV, Mikheenko A, Vollger MR, Altemose N,
646 Uralsky L, Gershman A, et al. 2022. The complete sequence of a human genome.
647 *Science* **376**: 44–53.
648 Nuttle X, Giannuzzi G, Duyzend MH, Schraiber JG, Narvaiza I, Sudmant PH, Penn O, Chiatante
649 G, Malig M, Huddleston J, et al. 2016. Emergence of a Homo sapiens-specific gene
650 family and chromosome 16p11.2 CNV susceptibility. *Nature* **536**: 205–209.
651 Perry GH, Dominy NJ, Claw KG, Lee AS, Fiegler H, Redon R, Werner J, Villanea FA, Mountain
652 JL, Misra R, et al. 2007. Diet and the evolution of human amylase gene copy number
653 variation. *Nat Genet* **39**: 1256–1260.
654 Pignatelli D, Carvalho BL, Palmeiro A, Barros A, Guerreiro SG, Macut D. 2019. The
655 Complexities in Genotyping of Congenital Adrenal Hyperplasia: 21-Hydroxylase
656 Deficiency. *Front Endocrinol* **10**.
657 Prodanov T, Bansal V. 2022. Robust and accurate estimation of paralog-specific copy number
658 for duplicated genes using whole-genome sequencing. *Nat Commun* **13**: 3221.
659 Sidransky E, Nalls MA, Aasly JO, Aharon-Peretz J, Annesi G, Barbosa ER, Bar-Shira A, Berg D,
660 Bras J, Brice A, et al. 2009. Multicenter analysis of glucocerebrosidase mutations in
661 Parkinson's disease. *N Engl J Med* **361**: 1651–1661.
662 Steyaert W, Haer-Wigman L, Pfundt R, Hellebrekers D, Steehouwer M, Hampstead J, de Boer
663 E, Stegmann A, Yntema H, Kamsteeg E-J, et al. 2023. Systematic analysis of
664 paralogous regions in 41,755 exomes uncovers clinically relevant variation. *Nat*

Commun **14**: 6845.
Swanepoel CM, Gerlinger ER, Mueller JL. 2020. Large X-Linked Palindromes Undergo Arm-to-Arm Gene Conversion across Mus Lineages. *Mol Biol Evol* **37**: 1979–1985.
ten Broeke SW, van der Klift HM, Tops CMJ, Aretz S, Bernstein I, Buchanan DD, de la Chapelle A, Capella G, Clendenning M, Engel C, et al. 2018. Cancer Risks for PMS2-Associated Lynch Syndrome. *J Clin Oncol* **36**: 2961–2968.
The 1000 Genomes Project Consortium. 2015. A global reference for human genetic variation. *Nature* **526**: 68–74.
Trombetta B, Cruciani F. 2017. Y chromosome palindromes and gene conversion. *Hum Genet* **136**: 605–619.
van der Klift HM, Tops CMJ, Bik EC, Boogaard MW, Borgstein A-M, Hansson KBM, Ausems MGEM, Garcia EG, Green A, Hes FJ, et al. 2010. Quantification of sequence exchange events between PMS2 and PMS2CL provides a basis for improved mutation scanning of lynch syndrome patients. *Hum Mutat* **31**: 578–587.
Vollger MR, Dishuck PC, Harvey WT, DeWitt WS, Guitart X, Goldberg ME, Rozanski AN, Lucas J, Asri M, Human Pangenome Reference Consortium, et al. 2023. Increased mutation and gene conversion within human segmental duplications. *Nature* **617**: 325–334.
Vollger MR, Guitart X, Dishuck PC, Mercuri L, Harvey WT, Gershman A, Diekhans M, Sulovari A, Munson KM, Lewis AP, et al. 2022. Segmental duplications and their variation in a complete human genome. *Science* **376**: eabj6965.
Wang T, Antonacci-Fulton L, Howe K, Lawson HA, Lucas JK, Phillippy AM, Popejoy AB, Asri M, Carson C, Chaisson MJP, et al. 2022. The Human Pangenome Project: a global resource to map genomic diversity. *Nature* **604**: 437–446.
Wernstedt A, Valtorta E, Armelao F, Togni R, Girlando S, Baudis M, Heinimann K, Messiaen L, Staehli N, Zschocke J, et al. 2012. Improved Multiplex Ligation-Dependent Probe Amplification Analysis Identifies a Deleterious PMS2 Allele Generated by Recombination with Crossover Between PMS2 and PMS2CL. *Genes Chromosomes Cancer* **51**: 819–831.
Yokota Y, Moteki H, Nishio S, Yamaguchi T, Wakui K, Kobayashi Y, Ohyama K, Miyazaki H, Matsuoka R, Abe S, et al. 2019. Frequency and clinical features of hearing loss caused by STRC deletions. *Sci Rep* **9**: 4408.
Zipfel PF, Edey M, Heinen S, Józsi M, Richter H, Misselwitz J, Hoppe B, Routledge D, Strain L, Hughes AE, et al. 2007. Deletion of complement factor H-related genes CFHR1 and CFHR3 is associated with atypical hemolytic uremic syndrome. *PLoS Genet* **3**: e41.

Supplemental information

Supplementary figures

715 Figure S1. Gene families with significant CN deviations across populations.

716 One archetype gene is selected to represent the name of each family.

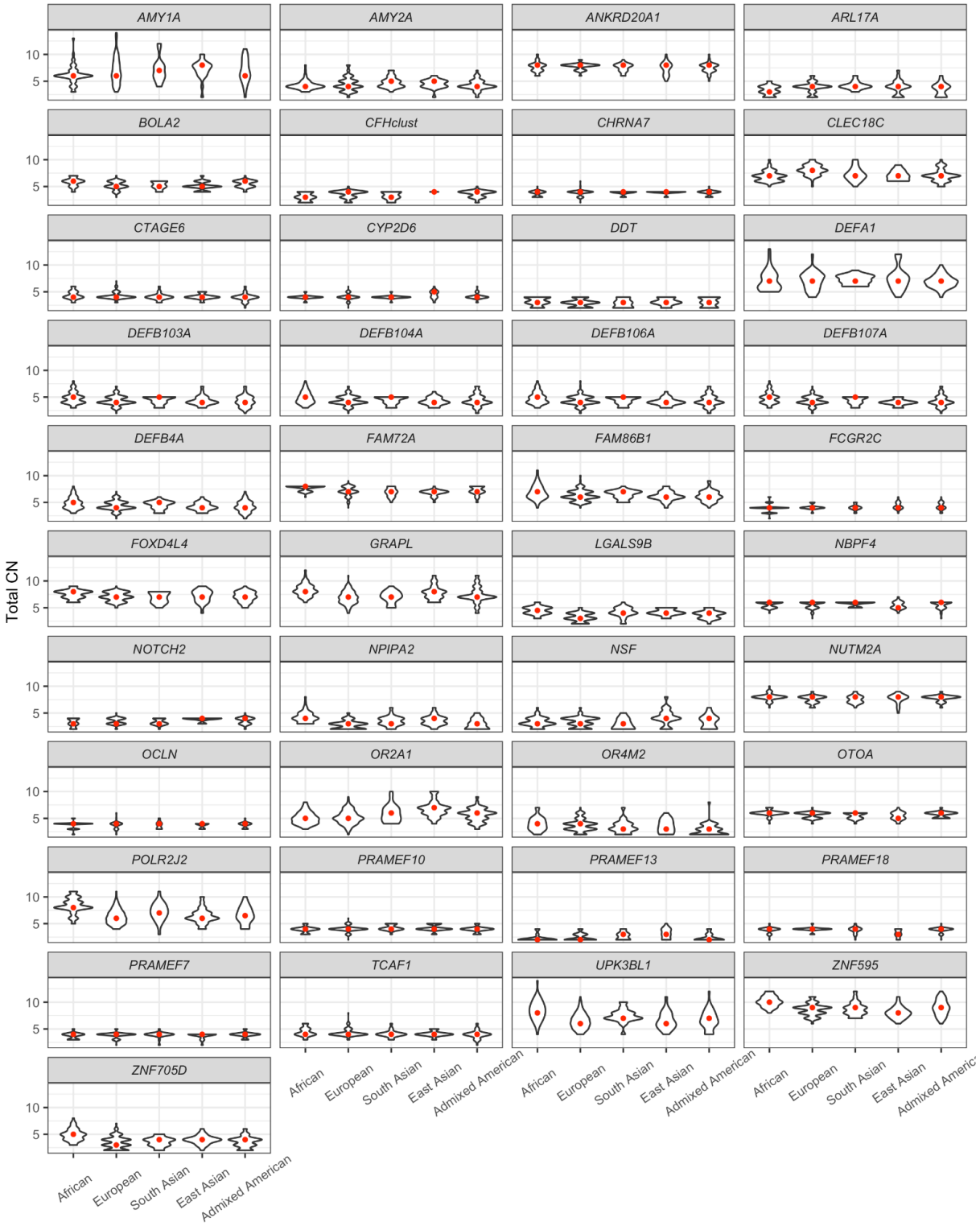

717

Figure S2. Paraphase results in false duplication regions with CHM13 data.

First three: false duplication regions not previously found in CHM13 T2T assembly (*DEFB109B*, *CNTNAP3/CNTNAP3C* and *POTED*).
Last three: regions erroneously assigned to false duplications by CHM13 T2T assembly (*CTAGE8/CTAGE9*, *OR2A1/OR2A42* and *RIMBP3/RIMBP3B/RIMBP3C*).

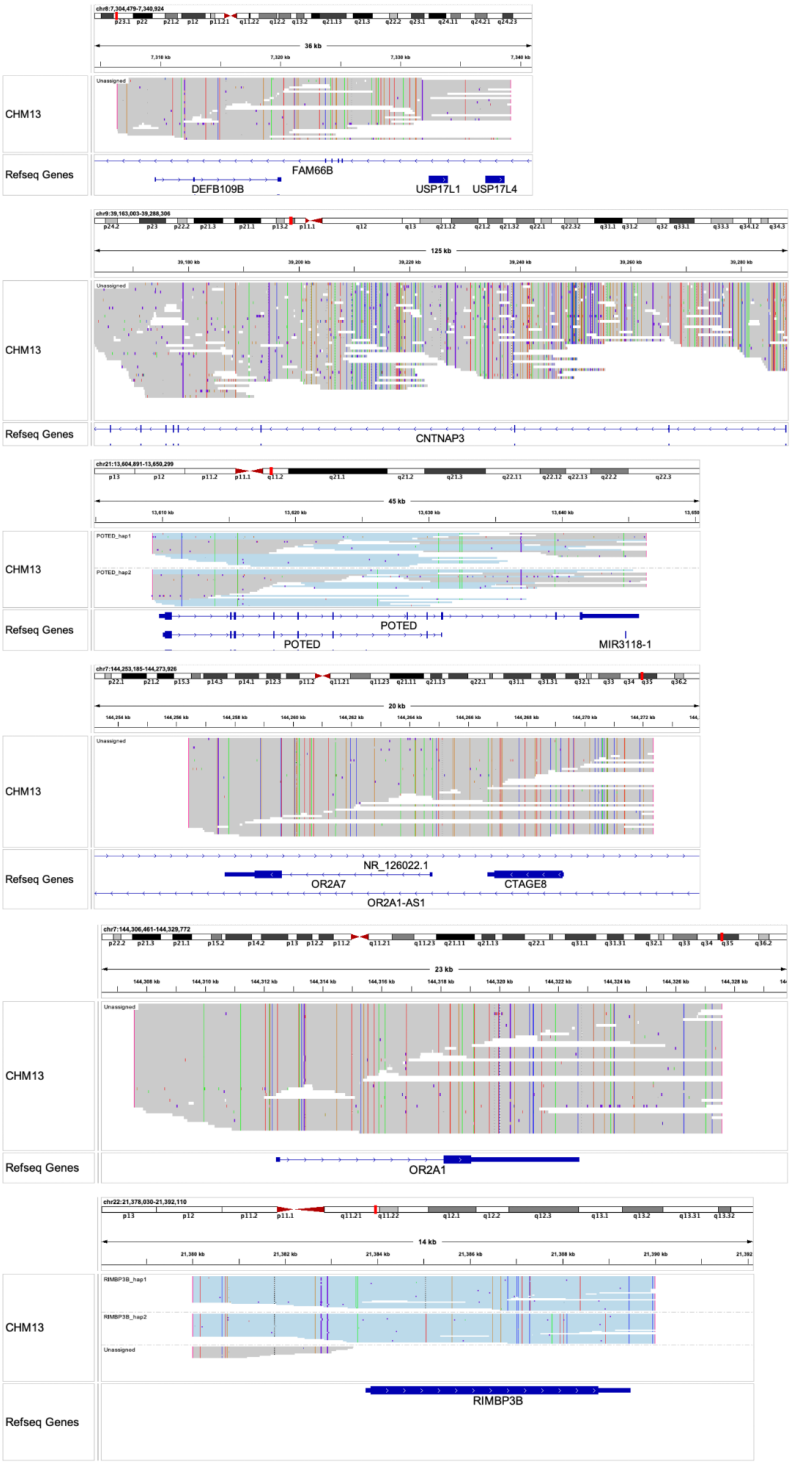

724 Figure S3. Principal component analysis (PCA) of Exons 1-6 and Exons 7-
725 8 sequences in *SMN1/SMN2*.

726 Exons 1-6 (A-C) sequences are highly similar to each other, with little variation explained by
727 each PC (A). *SMN1* and *SMN2* haplotype sequences do not separate into distinct clusters (B).
728 Instead, the separation on PC1 is by ancestry (C). Exons 7-8 (D-F) are more differentiated, with
729 a much higher level of variation explained by PC1 (D), which separates haplotype sequences by
730 gene (E) rather than ancestry (F).

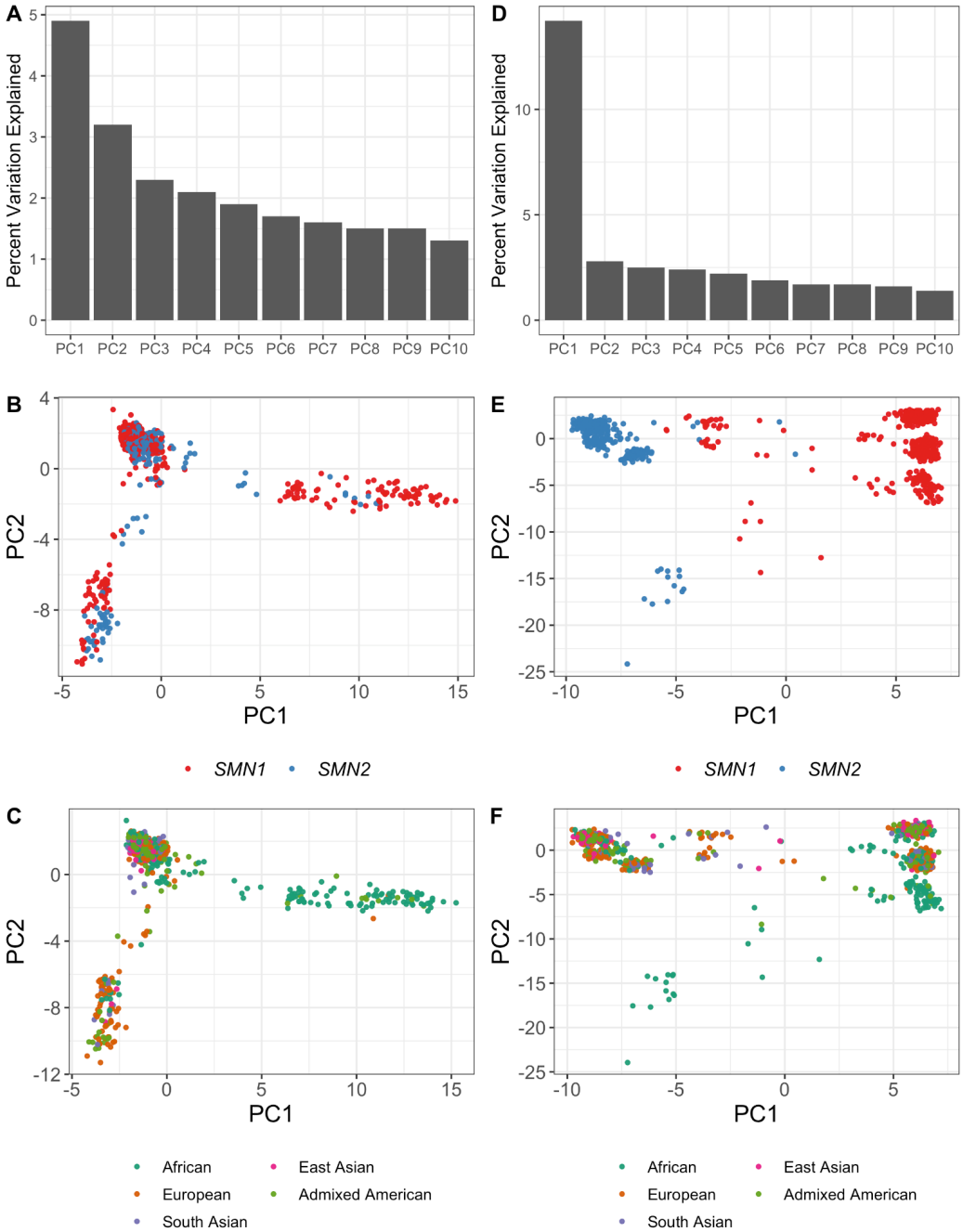

731

732 Figure S4. Histograms of pairwise sequence divergence for gene families
733 with differentiated genes and paralogs (upper panel) vs. gene families with
734 low within-family diversity (lower panel).

735 With differentiated genes in the same family, we expect to see two distinct peaks representing
736 low gene-gene (and paralog-paralog) sequence divergence and high gene-paralog sequence
737 divergence. On the other hand, in gene families with low within-family diversity, gene-gene (and
738 paralog-paralog) sequence divergence is similar to gene-paralog sequence divergence and they
739 do not form two peaks. RCCX contains *CYP21A2/CYP21A1P*, *C4A/C4B* and *TNXB/TNXA*.
740

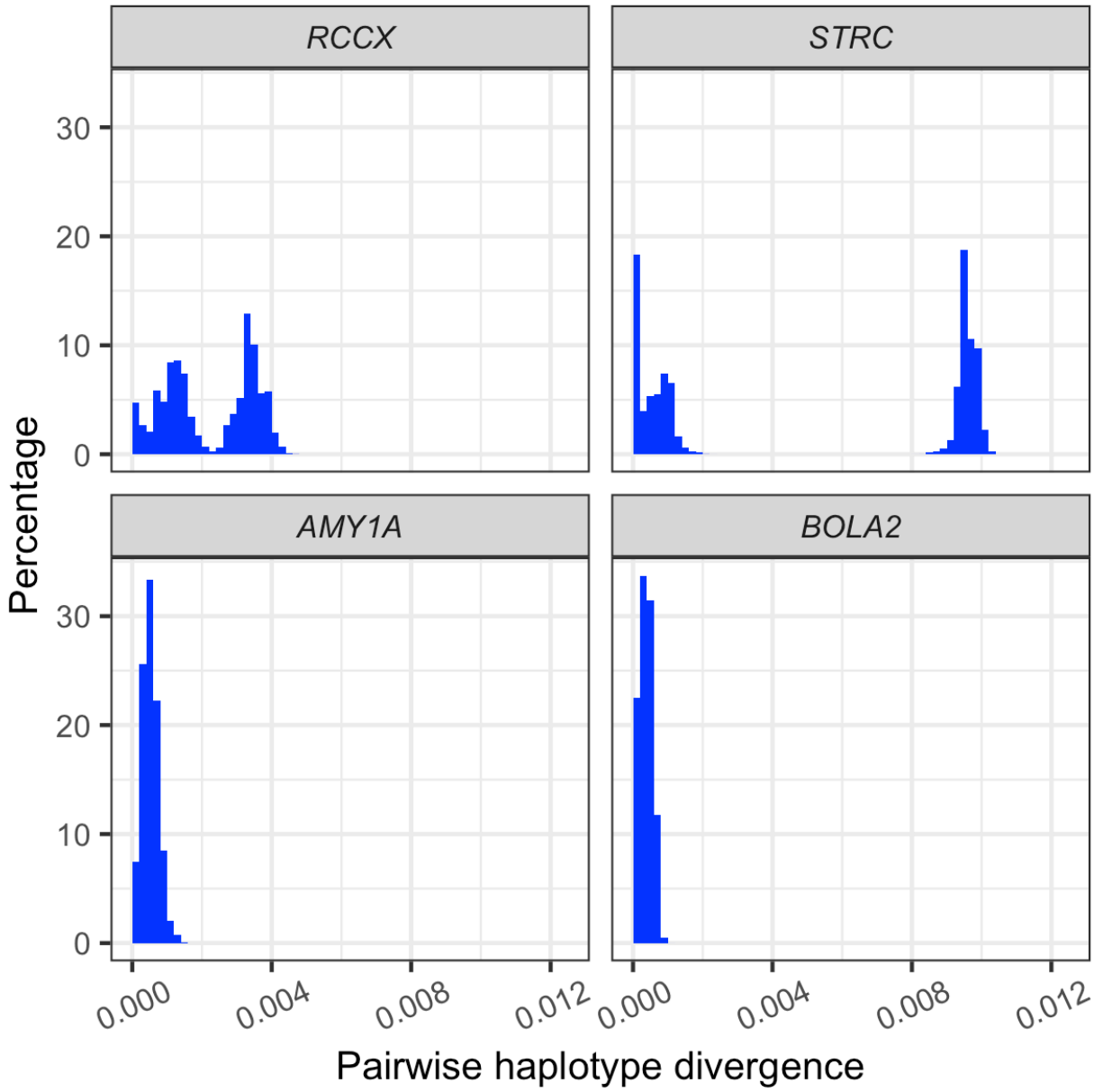

741
742

743 Figure S5. Details of PCA results shown in Figure 3B-D.

744 Each row shows the PCA results for one gene family.

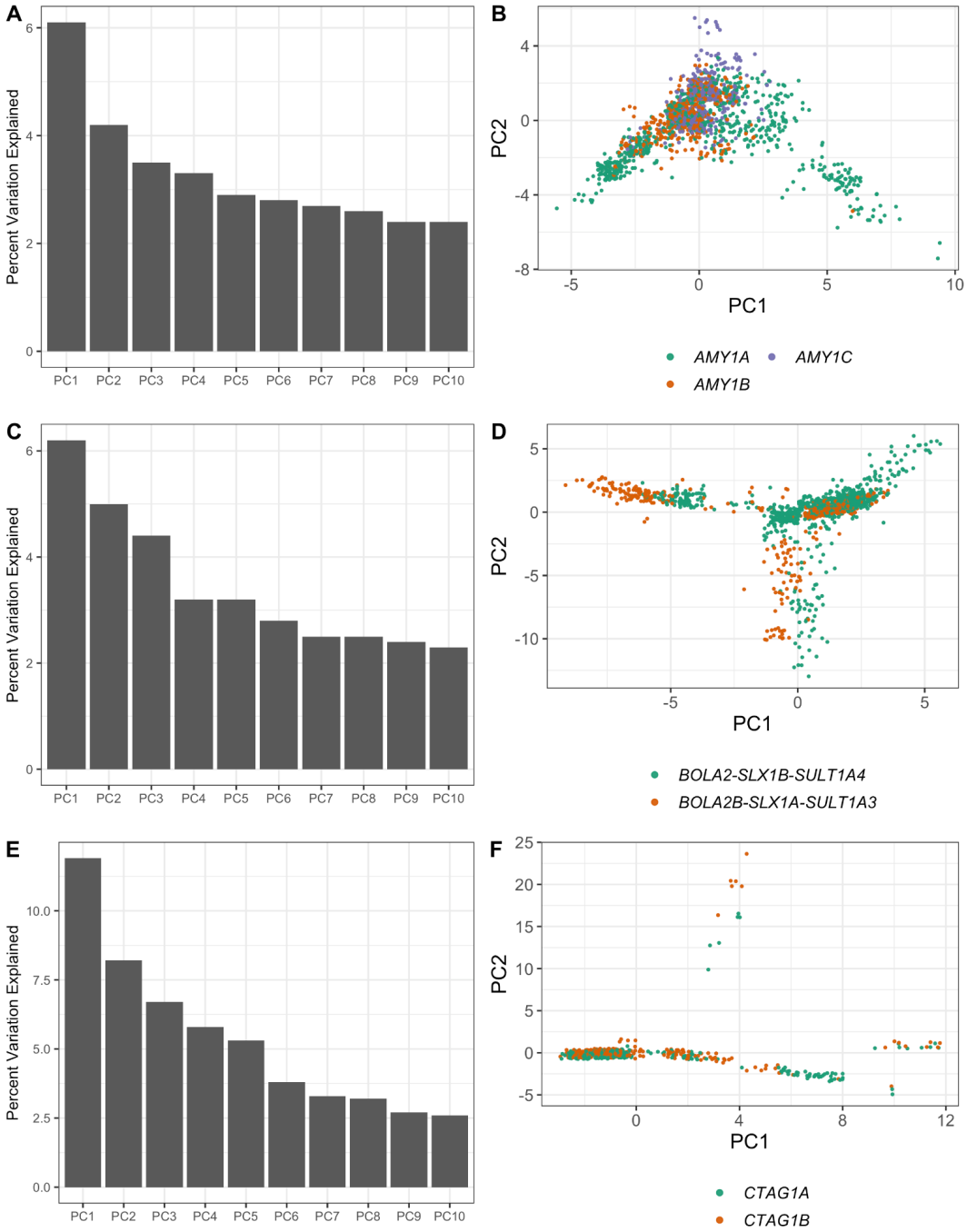

745
746

Figure S6. *De novo* SNV #1.

Variant is intergenic. Variant is marked by the black arrow. B is a close view of the variant.

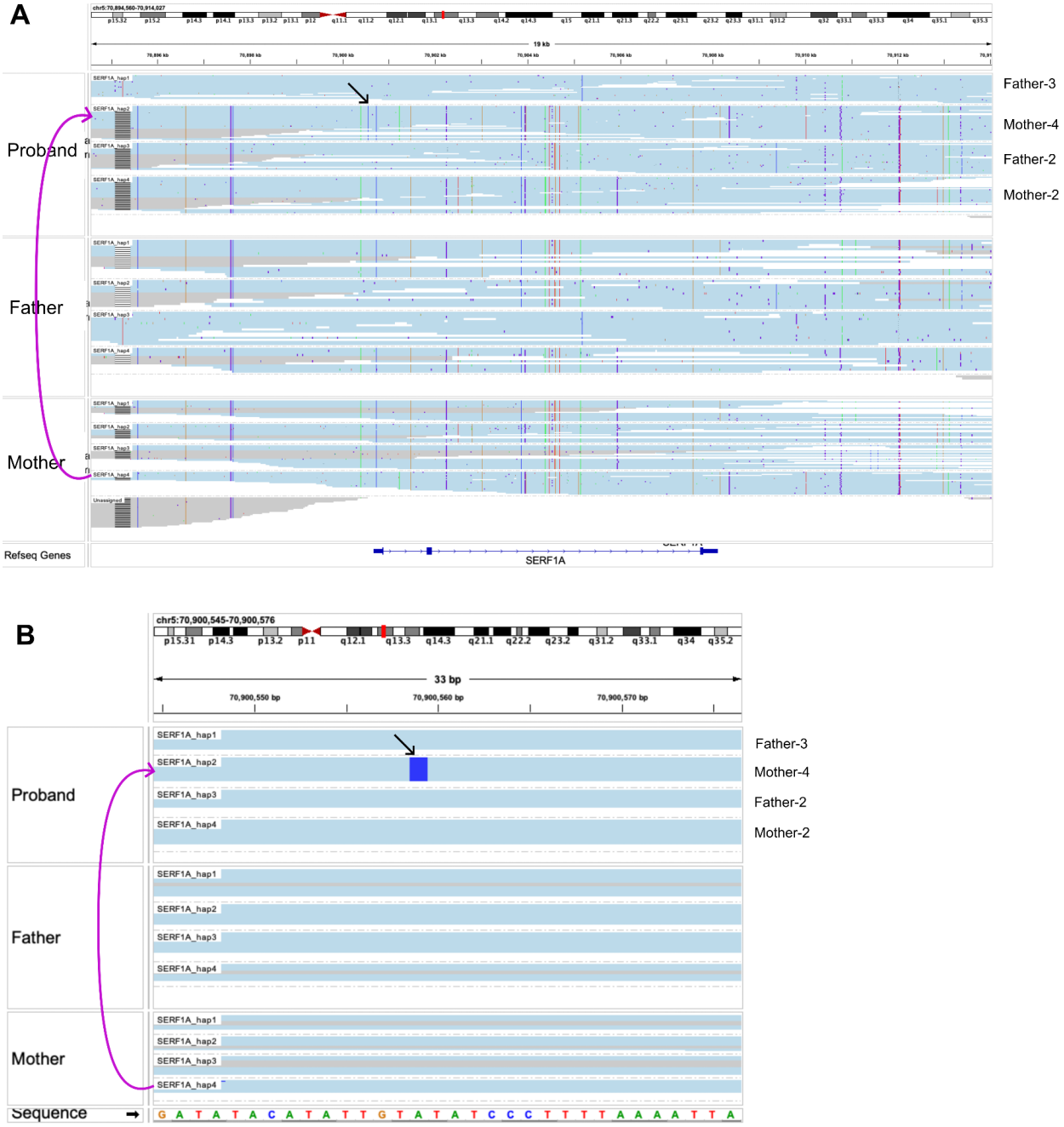

751 Figure S7. *De novo* SNV #2.

752 Variant is synonymous. Variant is marked by the black arrow. B is a close view of the variant.

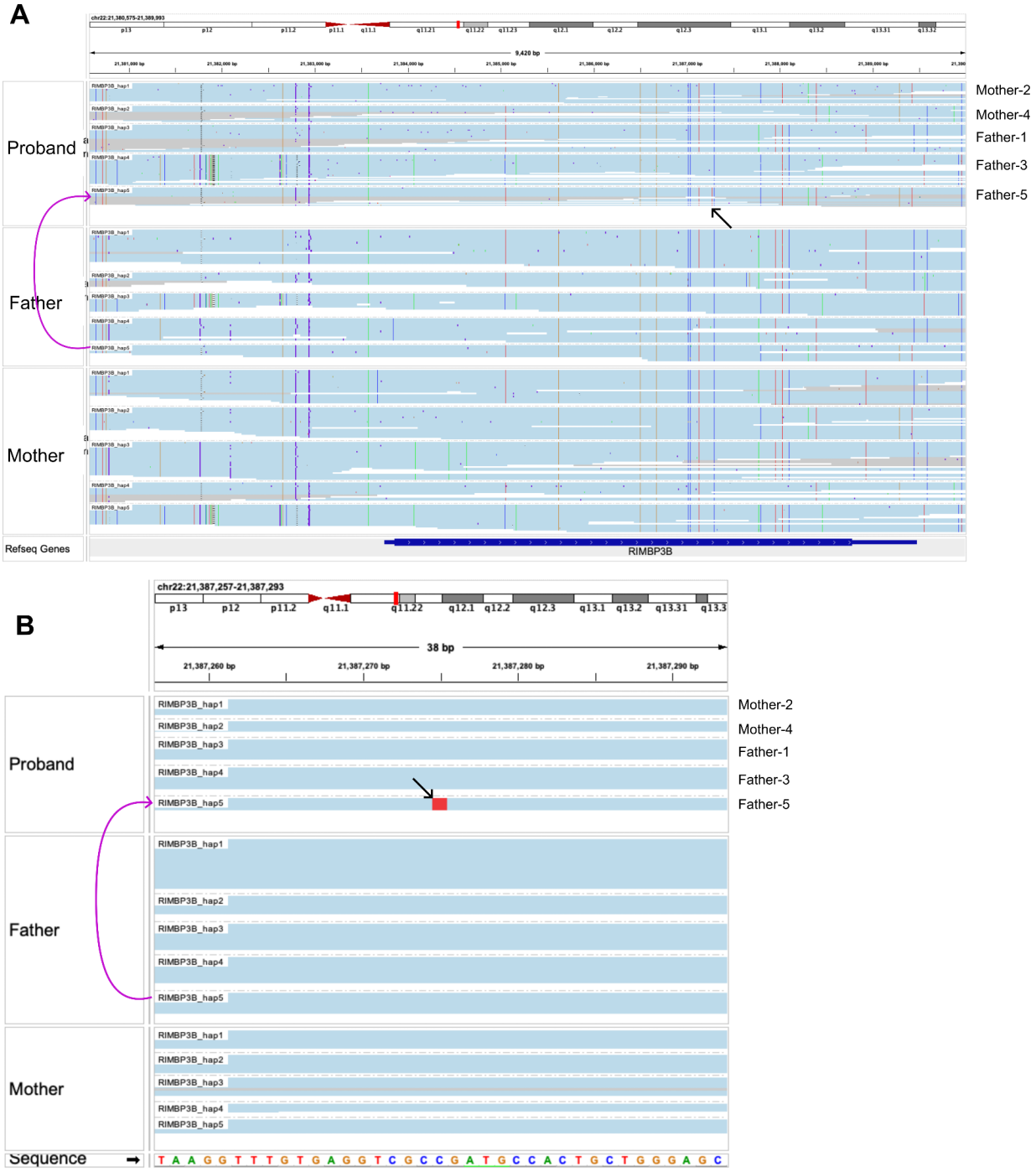

753

754

Figure S8. *De novo* SNV #3.

Variant is intergenic. Variant is marked by the black arrow. B is a close view of the variant.

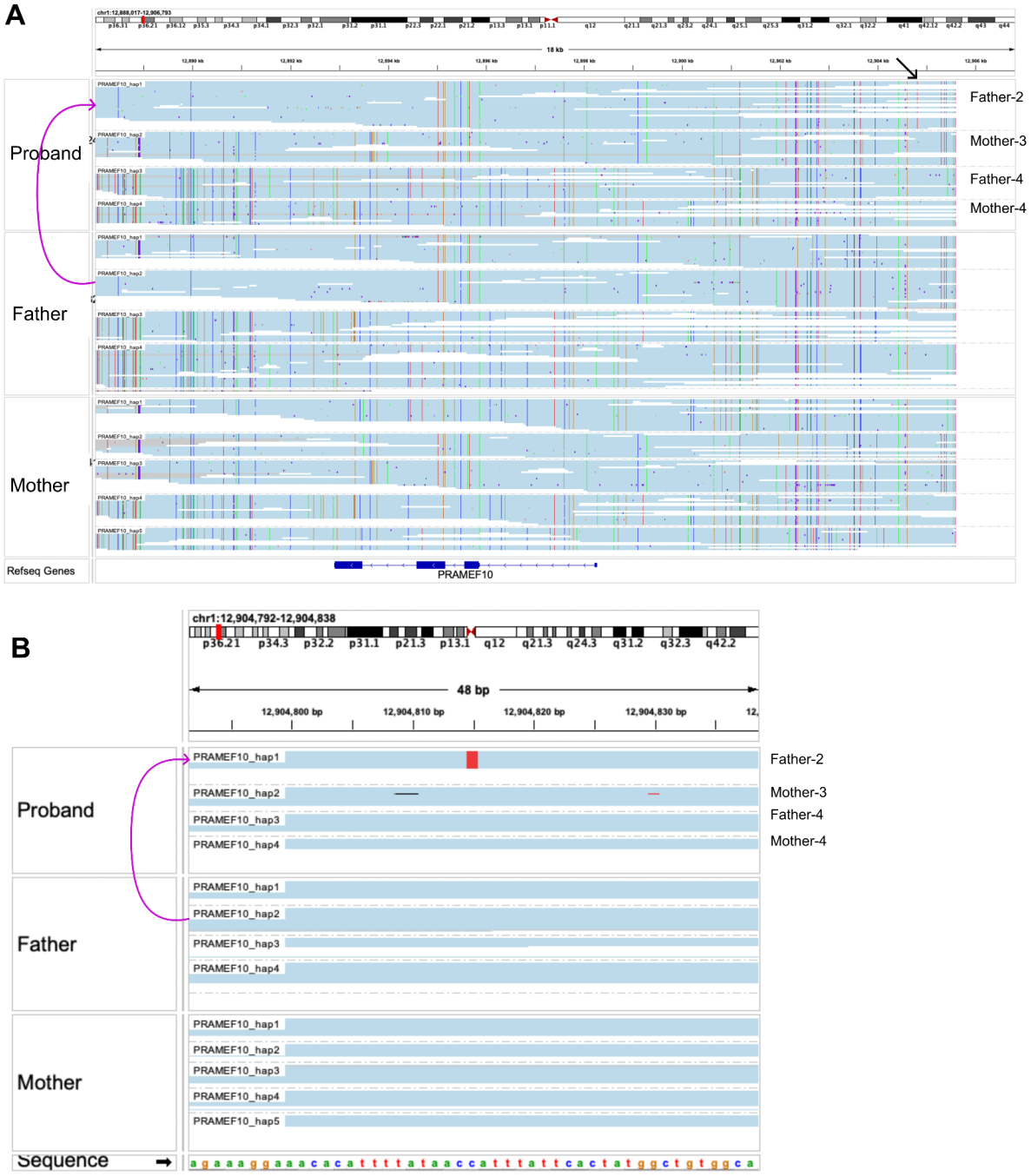

759 Figure S9. *De novo* SNV #4.

760 Variant is intronic. Variant is marked by the black arrow. B is a close view of the variant.

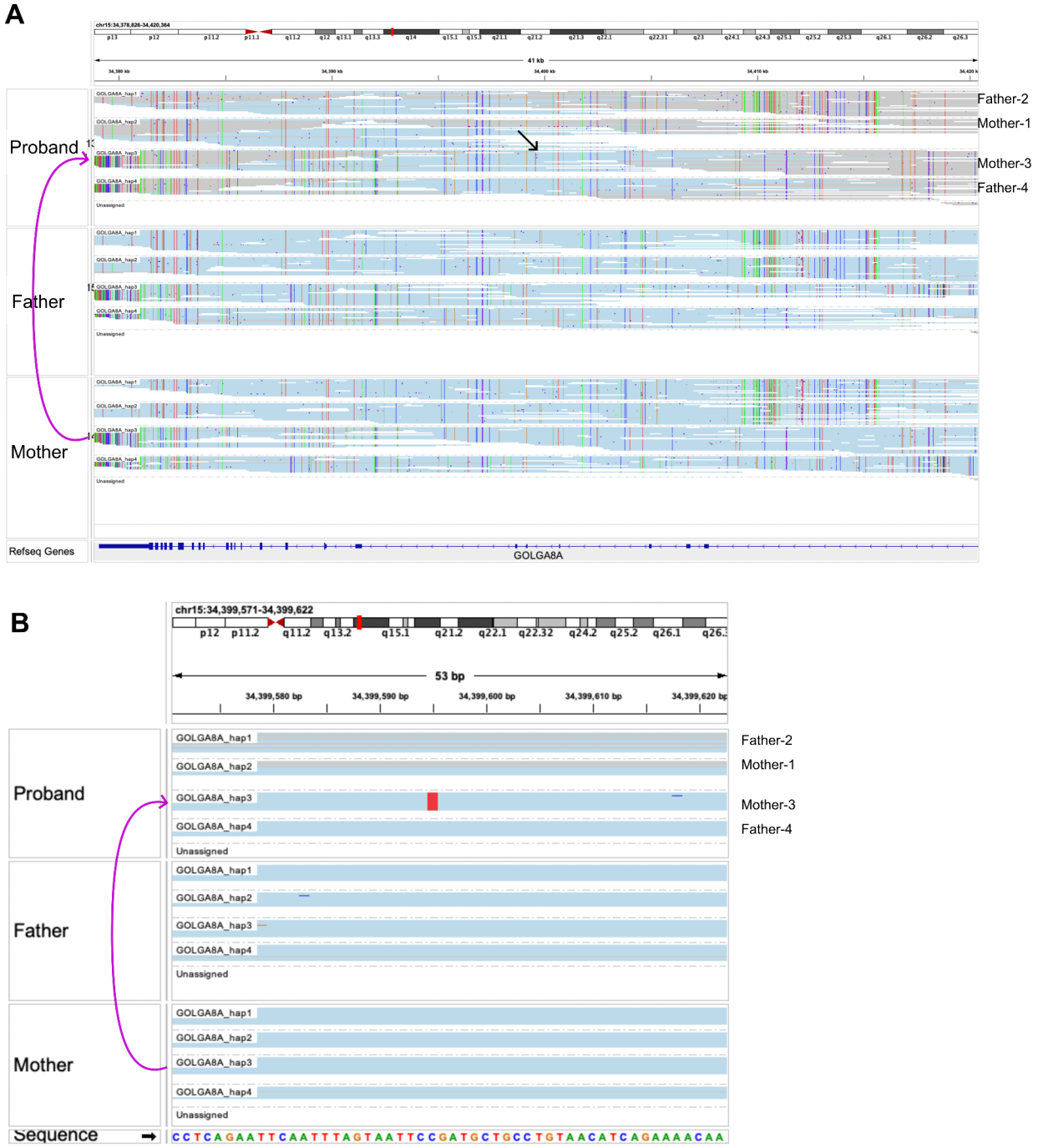

761

762

Figure S10. *De novo* SNV #5.

Variant is intergenic. Variant is marked by the black arrow. B is a close view of the variant.

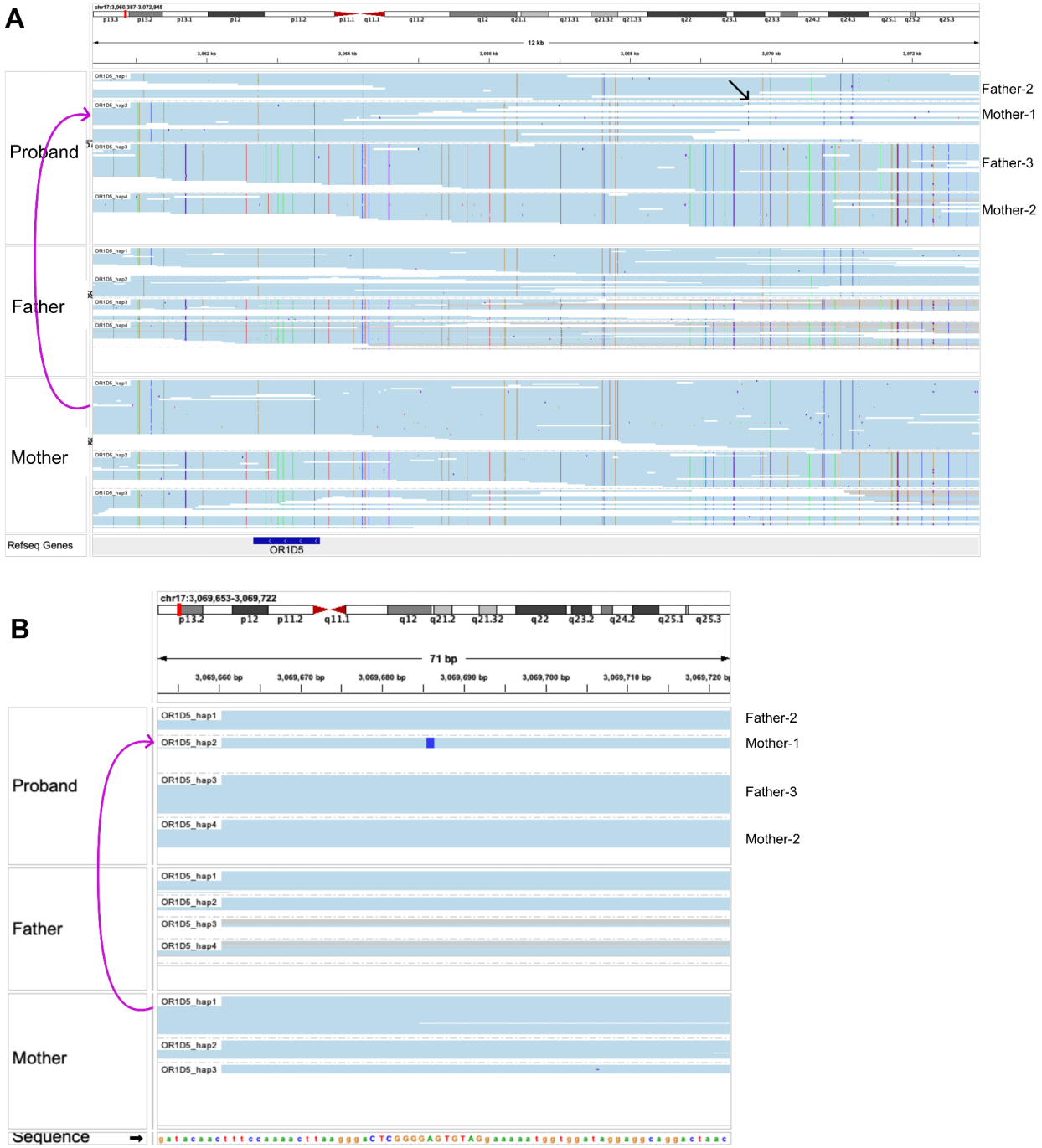

Figure S11. *De novo* SNV #6.

Variant is intronic. Variant is marked by the black arrow. B is a close view of the variant.

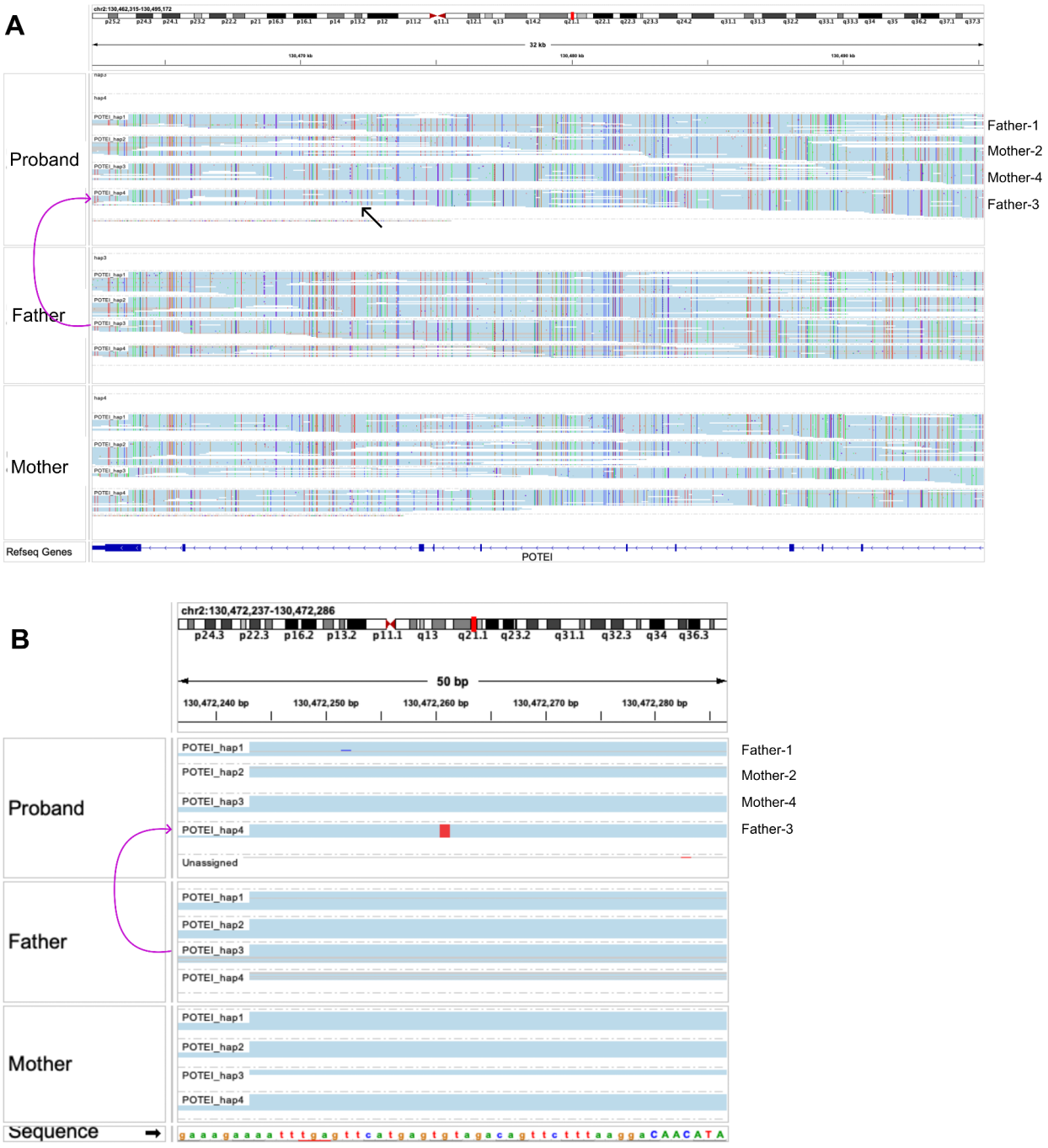

Figure S12. *De novo* SNV #7.

Variant is intronic. Variant is marked by the black arrow. B is a close view of the variant.

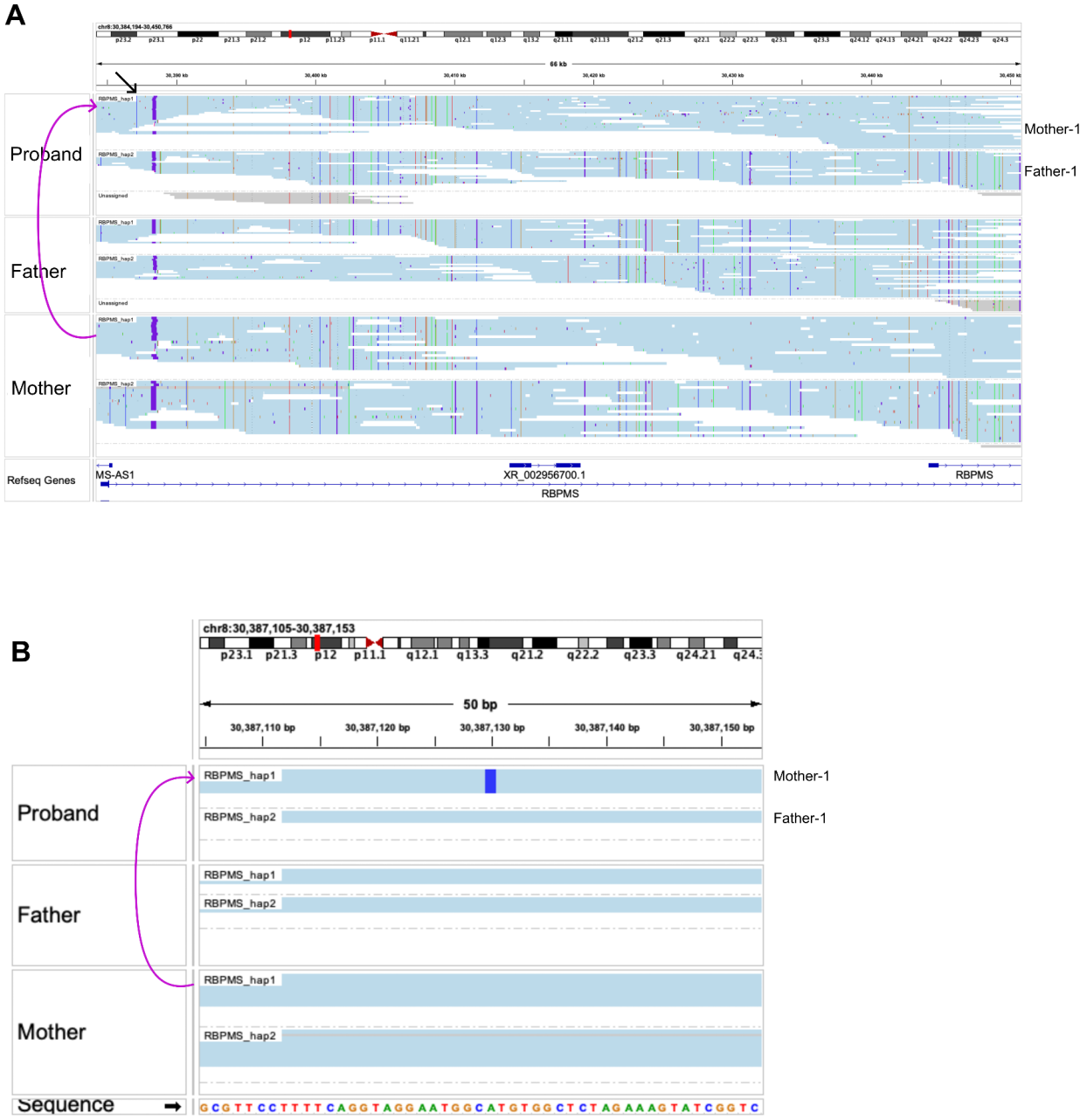

775 Figure S13. Non-allelic gene conversion #2 (in addition to Figure 4).

776 Variant is intronic. Black arrows mark the variant as well as the potential direction of conversion.

777 B is a close view of the variant.

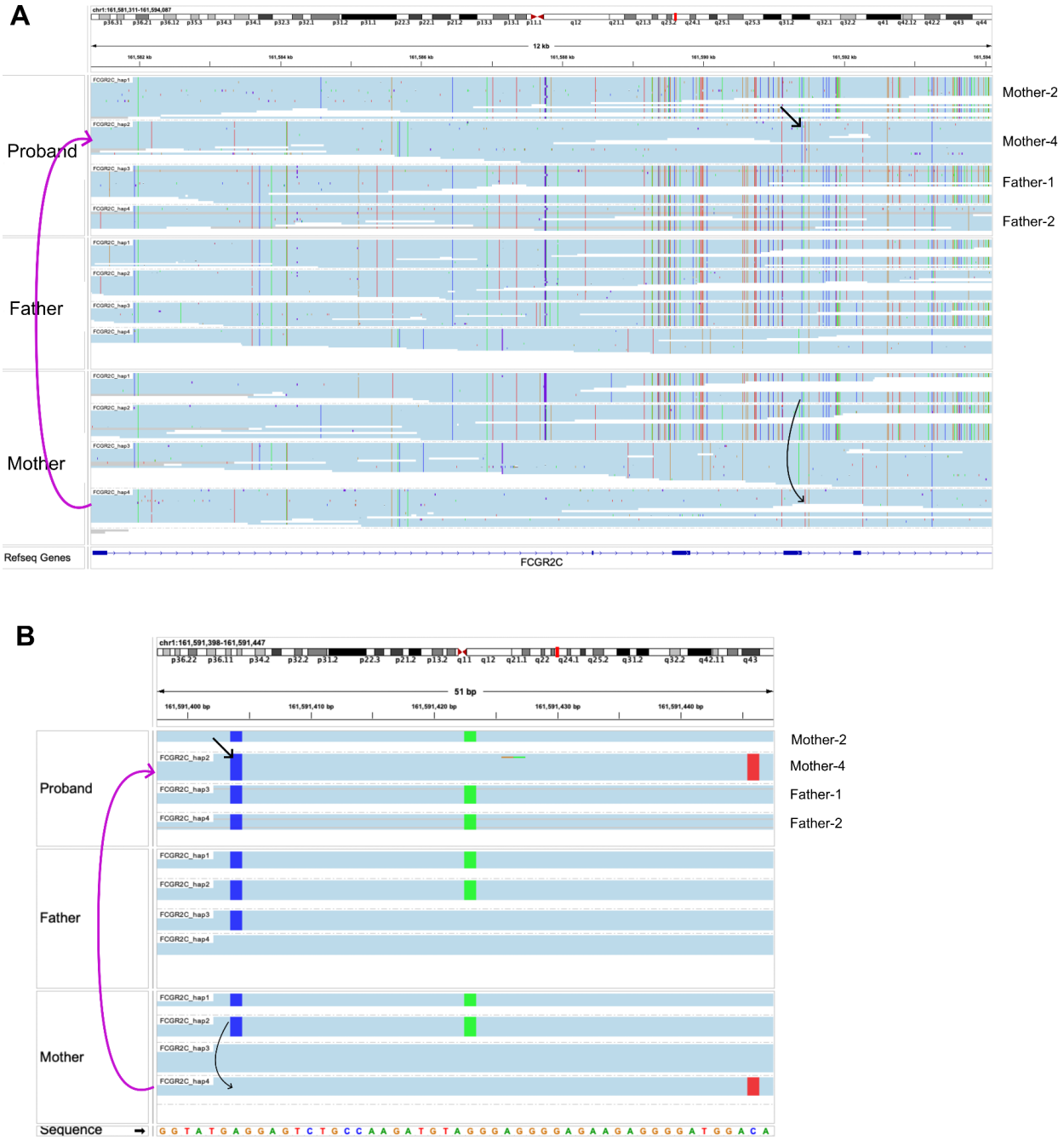

778

779

780 Figure S14. Allelic gene conversion.

781 Variant is intronic. Variant is marked by the black arrow. B is a close view of the variant.

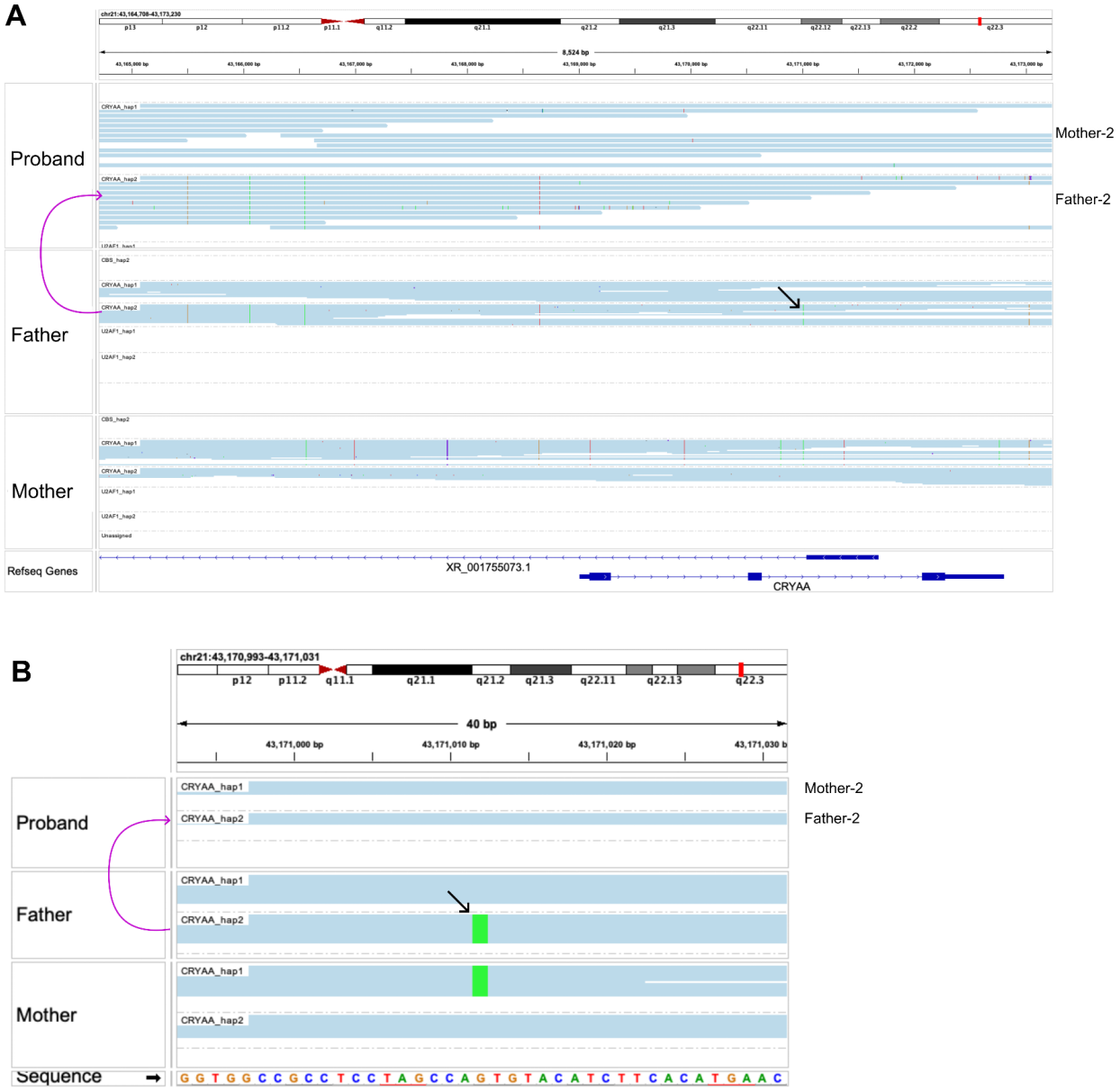

782

783

Figure S15. Gene conversion allelic/non-allelic.

Variant is intronic. Black arrows mark the variant as well as the potential direction of conversion. B is a close view of the variant.

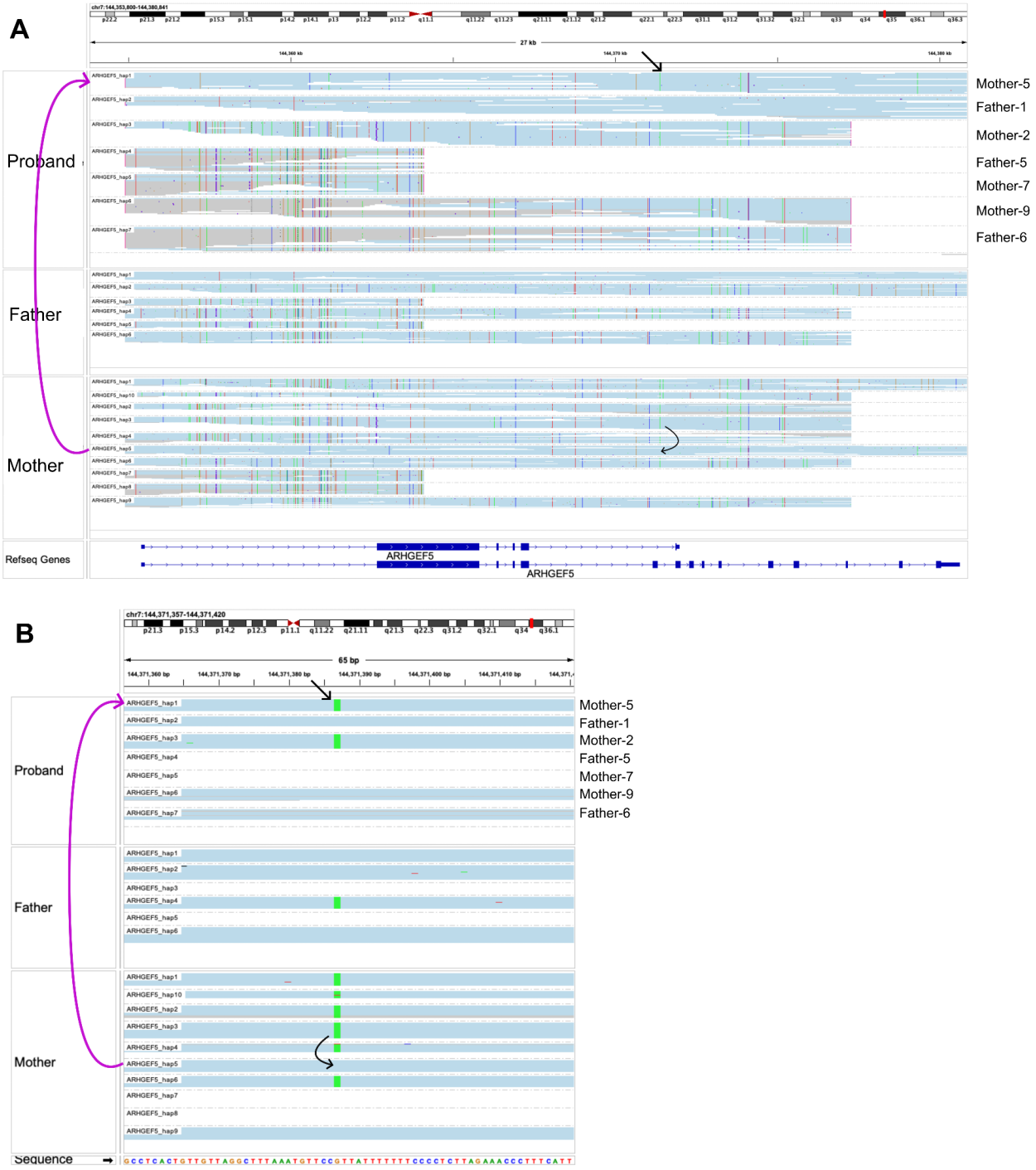

Figure S16. Hybrid haplotype due to equal or unequal crossing over.

The red and black boxes mark two parts of the hybrid haplotype and their origin in the father.

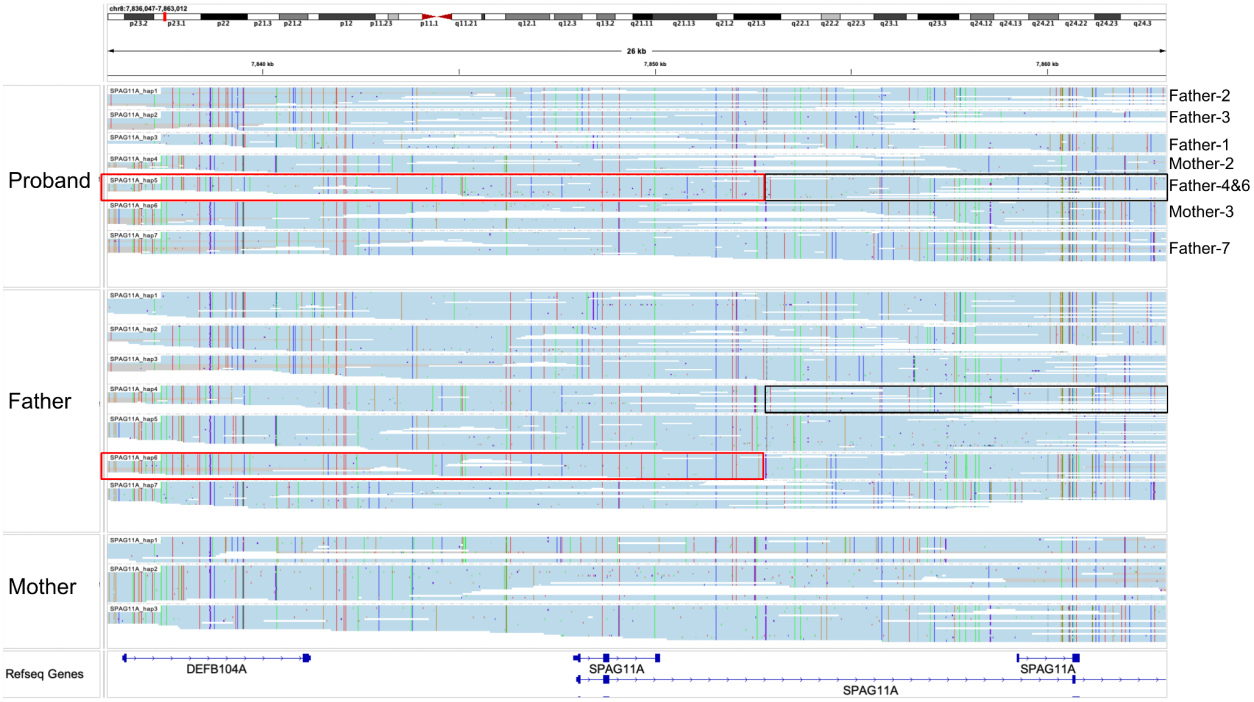

794 Figure S17. PCA of Exon12, Exon13-14 and Exon15 sequences in
795 *PMS2/PMS2CL*.

796 *PMS2* and *PMS2CL* are distinguishable in Exon 12 and Exons 13-14, with occasional gene
797 conversions. *PMS2* and *PMS2CL* are indistinguishable in Exon 15.

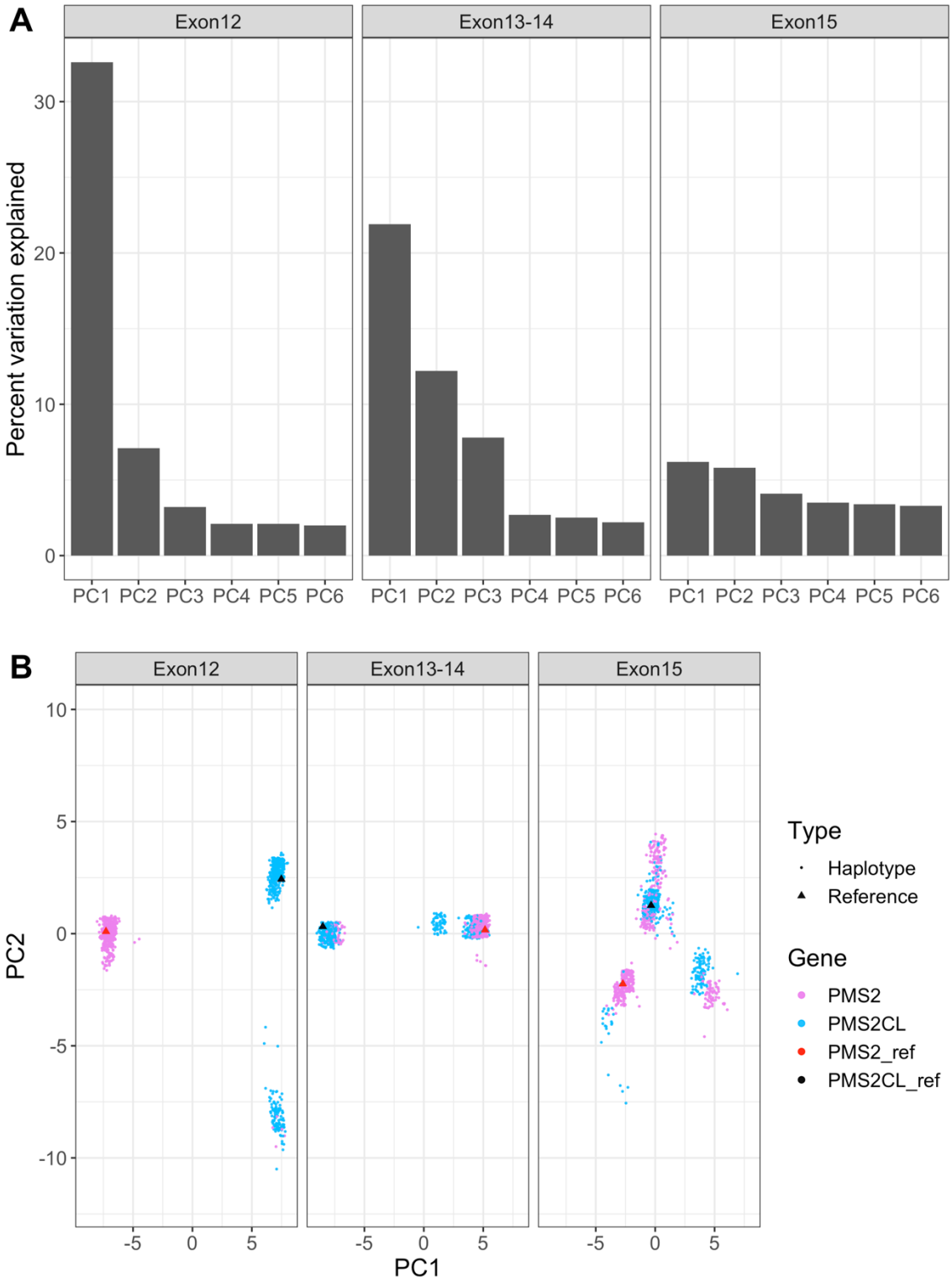

798

Figure S18. Distribution of the copy number of *SMN1* and *SMN2* across populations.

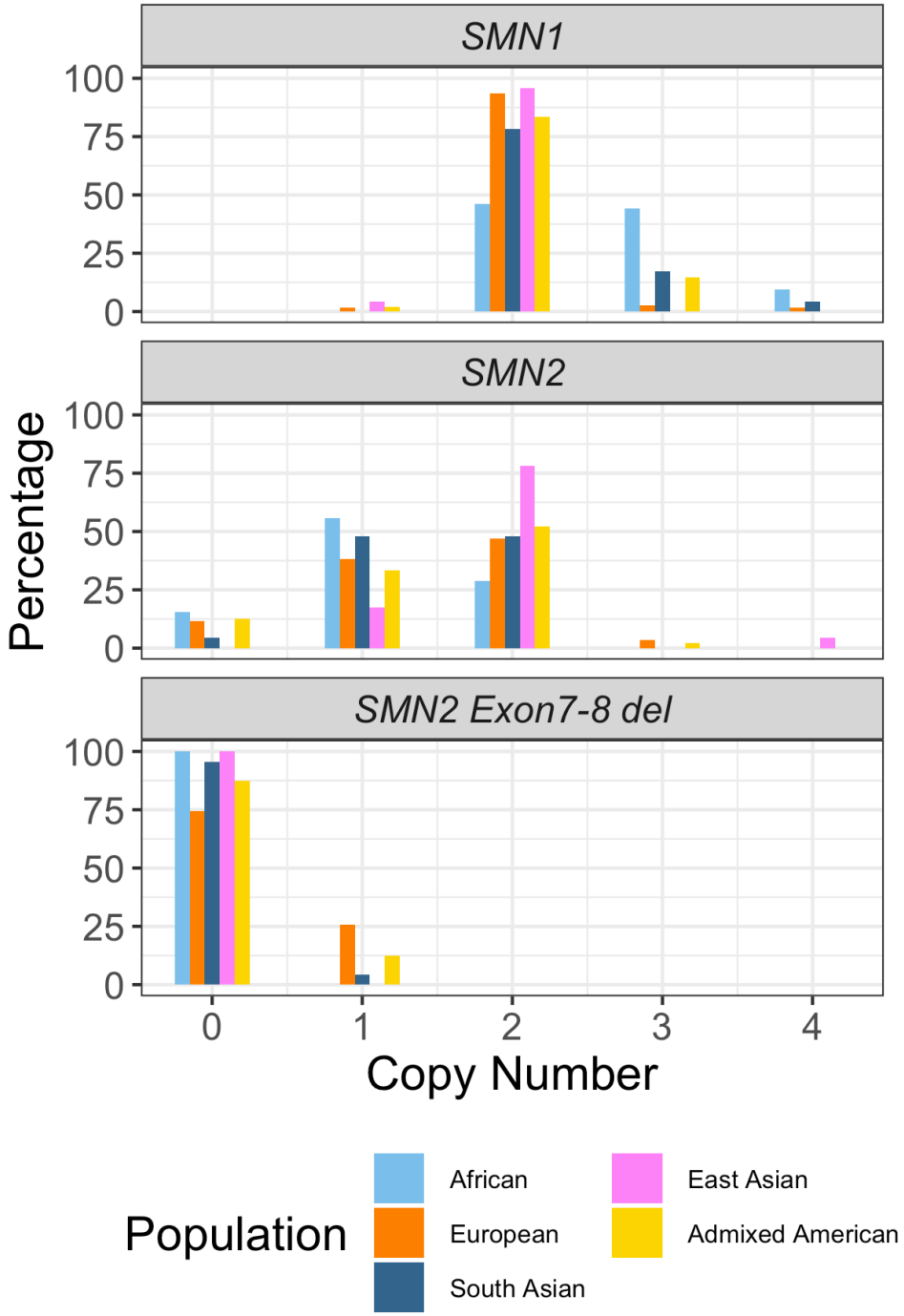

803 Figure S19. Distribution of the copy number of *STRC* across populations.

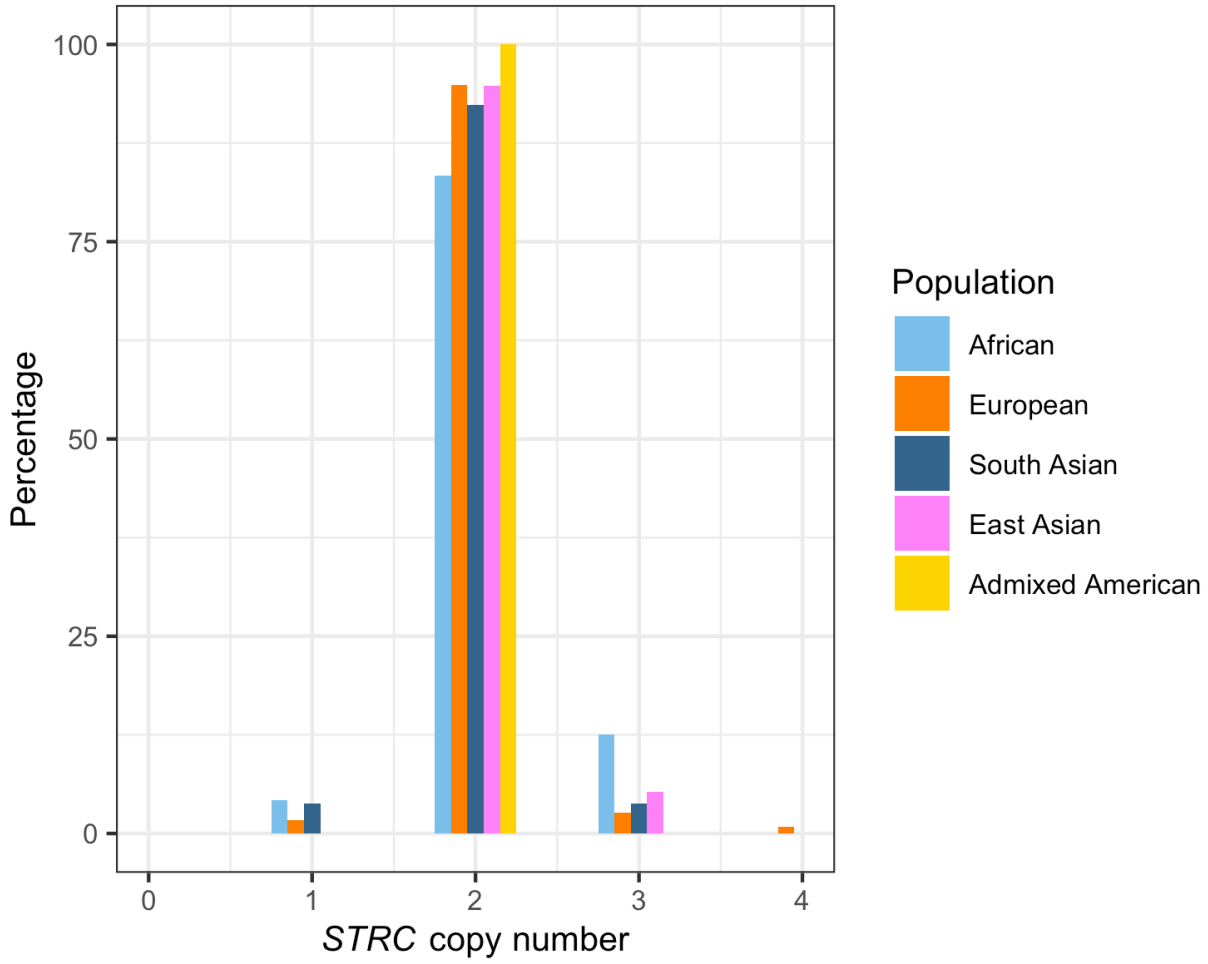

804

805 Figure S20. Distribution of the number of highly similar paralogs for genes
806 in SDs.

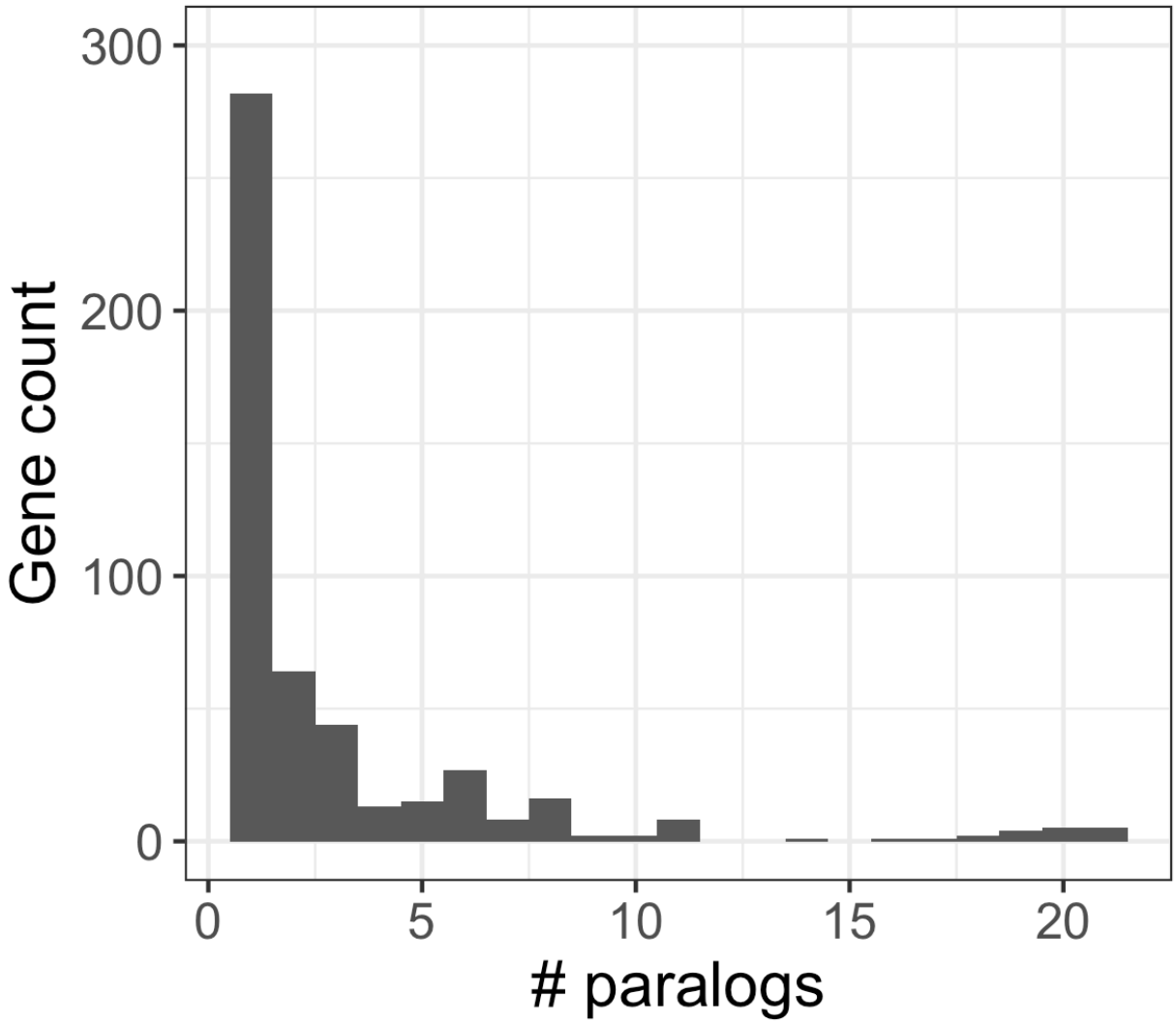

807
808

809 Figure S21. Distributions of allelic sequence divergence for genes without
810 paralogs

811 Distribution of pairwise sequence divergence between haplotypes among 400 randomly
812 selected autosomal genes and 200 randomly selected chrX genes. Red vertical lines represent
813 the 90th percentile.
814

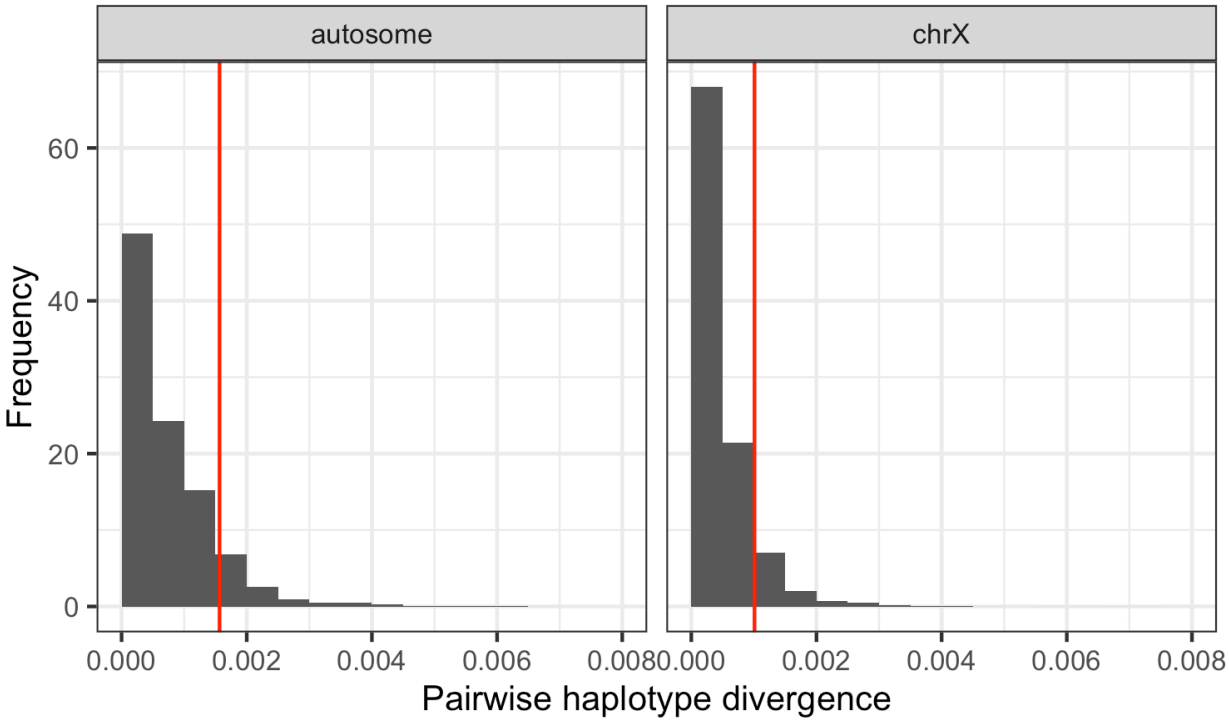

815
816
817

818 # Supplementary Tables

819 Table S1. Details on SD regions analyzed by Paraphase, including
820 summaries on CN variability and pairwise haplotype divergence (Excel
821 spreadsheet)

822 Table S2. Details on validation samples (Excel spreadsheet)

823

824 Table S3. Genes that fall in SDs in GRCh38 but have a consistent CN of
825 two across populations.

Genes	Coordinate in GRCh38	Other coordinate in GRCh38	% samples with CN>2	Previously known (Nurk et al. 2022)
DEFB130A/ DEFB130B	chr8:12304640-12323365	chr8:12058076-12076797	0.39%	x
RBPMS	chr8:30384041-30448023	chrX:37085009-37099262	0.39%	x
DEFB109B	chr8:7306410-7339183	chr8:7971187-8003955	0.78%	
CNTNAP3/ CNTNAP3C	chr9:39165433-39288814	chr9:61330217-61453530	2.7%	
MRPL23	chr11:1944688-1961966	chr11_KI270721v1_random:1-17145	0.39%	x
IQCK	chr16:19760000-19830000	chr13:86252980-86269524	1.16%	x
POTED	chr21:13609278-13646288	chrUn_GL000213v1:103302-140211	1.54%	
SMIM11	chr21:34374240-34392329	chr21:7743711-7761805	0.39%	x
C21orf140	chr21:34390593-34406217	chr21:7760069-7775696	0.39%	x
SMIM34	chr21:34411334-34431333	chr21:7781322-7801320	0.39%	x
KCNE1	chr21:34446191-34495759	chr21:7816178-7865746	1.16%	x
CBS	chr21:43052692-43076335	chr21:6444370-6468013	0	x
U2AF1	chr21:43090264-43110263	chr21:6481931-6501941	0	x
CRYAA	chr21:43160907-43173805	chr21:6552585-6565485	0	x
SIK1	chr21:43410808-43430807	chr21:6107453-6127452	0	x
HSF2BP	chr21:43528687-43659988	chr21:5966594-6009880	0.77%	x
TRAPPC10	chr21:44011809-44107052	chr21:5155001-5166246	1.17%	x
PWP2	chr21:44106900-44131681	chr21:5130371-5155153	0.39%	x
GATD3	chr21:44129698-44147864	chr21:5114188-5132354	0	x
ICOSLG	chr21:44221968-44241967	chr21:5021530-5041695	0.77%	x

DGCR6	chr22:18899205-18919204	chr22_KI270734v1_random:124478-144502	1.96%	x
PRODH	chr22:18912282-18936793	chr22_KI270734v1_random:137587-162092	1.93%	x

826

827 Table S4. *CYP21A2* allele frequencies

Allele	**African**	**European**	**South Asian**	**East Asian**	**Admixed American**
WT (*CYP21A2*, *CYP21A1P*)	80.2%	73.5%	74.0%	84.2%	78.9%
CYP21A1P deletion	11.5%	15.0%	6.0%	7.9%	13.2%
CYP21A1P duplication	3.1%	6.6%	16.0%	5.3%	6.6%
CYP21A2 duplication	1.0%				
CYP21A2(WT), *CYP21A2*(Q319X), *CYP21A1P*	1.0%	2.2%	2.0%		1.3%
Alleles carrying pathogenic *CYP21A2* variants, listed below	3.1%	2.5%	2.0%	2.6%	
M240K	1.0%				
Q319X		0.4%	2.0%		
V282L	2.1%	1.3%			
G111Vfs		0.4%			
Fusion deletion		0.4%			
Large conversion				2.6%	

828

829 Table S5. *OPN1LW/OPN1MW* allele frequencies

830

Allele (first two copies in the array)	**African**	**European**	**South Asian**	**East Asian**	**Admixed American**	**Phenotype**
OPN1LW+OPN1MW	96.2%	94.0%	96.3%	95.2%	93.9%	Normal
OPN1LW	1.3%			4.8%	1.5%	Deutan
OPN1LW+OPN1LW	2.5%	3.4%	3.7%		1.5%	
OPN1MW					1.5%	Protan
OPN1MW+OPN1MW		2.6%			1.5%	

831

832 Table S6. *HBA1/HBA2* allele frequencies

833

Allele	**African**	**European**	**South Asian**	**East Asian**	**Admixed American**
-a	11.5%	1.7%	5.9%	2.6%	3.7%
aa	88.5%	95.8%	92.2%	97.4%	93.9%
aaa		2.5%	2.0%		2.4%

834
835
836
837

838 Table S7. Frequencies of the deletion/duplication of the 11.7-kb region
839 (Exons 4-10) in *IKBKG/IKBKGP1.*
840

Gene	Allele	African	European	South Asian	East Asian	Admixed American
IKBKG	11.7-kb deletion					
	11.7-kb duplication		0.6%			
IKBKGP1	11.7-kb deletion		0.6%			3.2%
	11.7-kb duplication	5.1%	1.2%	2.8%		

841
842

843 Table S8. Deletion/Duplication frequencies in the *CFH* gene cluster.
844

SV (coordinates on chr1)	African	European	South Asian	East Asian	Admixed American
196748683_196833366_deletion	1.9%				
196760029_196844710_deletion	36.5%	20.2%	26.1%		18.8%
196792578_196917466_deletion		0.4%			
196813817_196935714_duplication		0.9%			
196815503_196937401_deletion	2.9%	0.4%			
196815503_196937401_duplication					1.0%

845
846

847 Table S9. Deletion/Duplication frequencies in the *GBA/GBAP1* region.

848

SV (coordinates on chr1)	**African**	**European**	**South Asian**	**East Asian**	**Admixed American**
155212923_155233549_deletion		0.4%			
155214276_155234903_duplication	5.8%				
155215100_155235727_duplication			2.2%		1.0%

849